

Enhancing lepton flavour violation in the supersymmetric inverse seesaw beyond the dipole contribution

Asmaa Abada*, Debottam Das†, Avelino Vicente‡ and Cédric Weiland§

Laboratoire de Physique Théorique, CNRS – UMR 8627,
Université Paris-Sud 11, F-91405 Orsay Cedex, France

Abstract

In minimal supersymmetric models the Z -penguin usually provides sub-dominant contributions to charged lepton flavour violating observables. In this study, we consider the supersymmetric inverse seesaw in which the non-minimal particle content allows for dominant contributions of the Z -penguin to several lepton flavour violating observables. In particular, and due to the low-scale (TeV) seesaw, the penguin contribution to, for instance, $\text{Br}(\mu \rightarrow 3e)$ and $\mu - e$ conversion in nuclei, allows to render some of these observables within future sensitivity reach. Moreover, we show that in this framework, the Z -penguin exhibits the same non-decoupling behaviour which had previously been identified in flavour violating Higgs decays in the Minimal Supersymmetric Standard Model.

KEYWORDS: Supersymmetry, Lepton Flavour Violation, Inverse Seesaw

*asmaa.abada@th.u-psud.fr

†debottam.das@th.u-psud.fr

‡avelino.vicente@th.u-psud.fr

§cedric.weiland@th.u-psud.fr

1 Introduction

In recent years, lepton physics has experienced an unprecedented experimental development. A non-vanishing - even unexpectedly large - value of the Chooz angle ($\theta_{13} \simeq 9^\circ$) has recently been measured by several (independent) collaborations [1–5]. Such a value of θ_{13} opens the door to very appealing phenomenological possibilities, among which CP violation in the leptonic sector stands as the best example. In parallel to these achievements, the other neutrino oscillation parameters (solar and atmospheric) are being determined with very good precision [6, 7]. In the near future, one does expect to identify the fundamental ingredients of flavour violation in the neutral lepton sector, but on the other hand, flavour violation in the charged lepton sector still remains to be observed. The present and future generations of high-intensity facilities dedicated to discovering flavour violation in charged lepton processes render feasible the observation of such an event in the near future.

Despite the fact that minimal extensions of the Standard Model (SM) can easily accommodate lepton flavour violation in the neutral lepton sector (i.e. neutrino oscillations), the contributions of these models to charged lepton flavour violating (cLFV) observables are typically extremely small. On the other hand, when such models - for example, the seesaw in its different realisations - are embedded within a larger framework, one can expect large contributions to cLFV observables, well within experimental reach. This is the case of supersymmetric versions of the seesaw mechanism, which in addition to apport solutions to many theoretical and phenomenological issues, such as the hierarchy problem, gauge coupling unification and dark matter, can also account for neutrino data.

However, these scenarios have several caveats, the most upsetting one being that they prove to be extremely hard to test, and thus can be neither confirmed nor excluded. This stems from the fact that in order to have sufficiently large Yukawa couplings (as required to account for large cLFV branching ratios), the typical scale of the extra particles (such as right-handed neutrinos, scalar or fermionic isospin triplets) is in general very high, potentially close to the gauge coupling unification scale.

This can be avoided if one simultaneously succeeds in having TeV-scale mediators, while preserving the possibility of large Yukawa couplings. From an effective theory point of view this is equivalent to the decoupling of the coefficients associated to the dimension-five (at the origin of neutrino masses) and dimension-six operators (for instance, four-fermion operators): in other words, decoupling the smallness of the light neutrino masses from the flavour violation sources. For instance, this is possible in the case of the type-II seesaw (and its supersymmetric (SUSY) realisations), as well as in the case of the so-called "inverse seesaw" (and the SUSY inverse seesaw).

The inverse seesaw [8] constitutes a very appealing alternative to the "standard" seesaw realisations, and has recently been the subject of several dedicated studies [9–21]. The inverse seesaw can be embedded in the Minimal Supersymmetric extension of the SM (MSSM) by the addition of two extra gauge singlet superfields, with opposite lepton numbers (+1 and -1). As extensively discussed in [9–21], in this framework one can in principle have large neutrino Yukawa couplings ($Y_\nu \sim \mathcal{O}(1)$) compatible with a seesaw scale, M_{seesaw} , close to the electroweak one (and thus within LHC reach), implying that there will be a significant enhancement of cLFV observables. This has fuelled a number of studies focusing on the potentialities of the inverse seesaw regarding cLFV and other phenomenological issues [9–12, 14–17, 21–24]. As recently discussed [25], the contributions of the comparatively light right-handed sneutrinos can enhance the Higgs-mediated penguin diagrams, leading to an augmentation of some observables - for instance $\text{Br}(\tau \rightarrow 3\mu)$ - by as much as two orders of magnitude, and have a non-negligible impact on Higgs-mediated leptonic B-meson decays and Higgs flavour violating decays.

These unique features - when compared to other SUSY seesaw realisations - open the door to rich phenomenological signatures, that can be potentially tested in the near future. The different high- and low-energy phenomenological implications of this class of models constitute the starting point to unveil the underlying mechanism of lepton mixing.

There are currently a large number of facilities [26–34], dedicated to the search of processes such as rare radiative decays, 3-body decays and muon-electron conversion in nuclei. Likewise, rare leptonic and semi-leptonic meson decays also offer a rich testing ground to experimentally probe cLFV.

These (low-energy) searches are complementary to the LHC which, in addition to directly searching for new physics states, also allow to study numerous signals of cLFV at high-energy, typically in association with neutralino-slepton decay chains. In order to disentangle the underlying model of lepton flavour violation, one relies on numerous strategies based on the interplay of low- and high-energy cLFV observables (see for example [35–38]). However, there are other avenues that can be explored in this quest to disentangle the underlying mechanism of neutrino mass generation, at the origin of lepton flavour violation: this approach is based upon exploring the correlation (or lack thereof) between different, unrelated, low-energy cLFV observables. The distinctive features of the underlying model will be manifest in the nature and specific hierarchy of the different contributions. For instance, in SUSY models where γ -penguins provide the dominant contribution to radiative and 3-body cLFV decays, one expects a strict correlation between $\text{Br}(\mu \rightarrow e\gamma)$ and $\text{CR}(\mu - e, \text{N})$. This is the case of constrained Minimal Supersymmetry Standard Model (cMSSM) based scenarios where additional lepton flavour violating sources have been introduced. Deviations from strict universality (as is the case of non-universal Higgs masses, NUHM), where for example Higgs-mediated penguins might play a significant rôle in $\mu - e$ conversion, break this strict correlation [39].

Independently of the specific mechanism of SUSY breaking, specific contributions to cLFV observables manifest a peculiar behaviour. A very interesting case is that of the Z -penguin: in the MSSM, the contributions of the Z -penguin to cLFV observables (such as $\ell_i \rightarrow 3\ell_j$ and $\mu - e$ conversion in nuclei) are suppressed by a subtle cancellation between the different terms in the amplitude. However, it has recently been noticed [40] that in models where new couplings are present or where the particle content is larger than that of the MSSM, the cancellation no longer holds, and the Z -penguin contributions can in fact provide the dominant contributions to cLFV processes such as 3-body decays, $\ell_i \rightarrow 3\ell_j$ and $\mu - e$ conversion in heavy nuclei. Models with additional couplings (as is the case of trilinear R-parity violating supersymmetric models) were discussed in [40, 41].

Contrary to the "standard SUSY seesaw", in the inverse SUSY seesaw the new states (in addition to those of the MSSM) do not decouple: indeed, the sterile states can be as light as to lie in the sub-GeV scale. In the framework of the inverse SUSY seesaw, one can see that the Z -penguins will also provide sizeable, if not dominant, contributions to a number of cLFV observables.

In this work, we consider a realisation of the inverse seesaw, embedding it into an otherwise lepton flavour conserving supersymmetric extension of the SM, the cMSSM. We conduct a detailed study of the impact that enhanced Z -penguins might have on a large number of low-energy cLFV observables, in particular $\mu - e$ conversion and $\mu \rightarrow 3e$ decay which in addition to being greatly enhanced by the Z -penguin, also have the best experimental prospects concerning the expected future sensitivities. Our results reveal that for vast regions of the parameter space, many cLFV observables are indeed boosted by the unsuppressed Z -penguin contribution and are within reach of present and future experiments.

Moreover, our analysis reveals that, similarly to what occurs in the MSSM, flavour changing Higgs boson decays (where the Higgs boson contributions do not decouple with increasing supersymmetric masses [42–44]), the Z -penguin contributions to the LFV observables are not suppressed by a large SUSY scale.

The paper is organised as follows: in Section 2, we will define the model, providing a brief overview on the implementation of the inverse seesaw in the MSSM. In Section 3, we discuss the enhancement of the Z -boson mediated contributions to low-energy cLFV observables. We also derive an analytical approximation for the $Z - \ell_i - \ell_j$ effective vertex. In Section 4, we derive analytical expressions for several cLFV observables in the case where Z -boson penguin is the dominant contribution. In Section 5, we detail the corresponding numerical study, collect the relevant numerical results and discuss the results as well as the decoupling regime. Our final remarks are given in Section 6.

2 Inverse seesaw mechanism in the MSSM

The inverse seesaw model consists of a gauge singlet extension of the MSSM. Three pairs of singlet superfields, $\widehat{\nu}_i^c$ and \widehat{X}_i ($i = 1, 2, 3$)¹ with lepton numbers assigned to be -1 and $+1$, respectively, are added to the superfield content. The SUSY inverse seesaw model is defined by the following superpotential

$$\begin{aligned} \mathcal{W} = \varepsilon_{ab} & \left[Y_d^{ij} \widehat{D}_i \widehat{Q}_j^b \widehat{H}_d^a + Y_u^{ij} \widehat{U}_i \widehat{Q}_j^a \widehat{H}_u^b + Y_e^{ij} \widehat{E}_i \widehat{L}_j^b \widehat{H}_d^a \right. \\ & \left. + Y_\nu^{ij} \widehat{\nu}_i^c \widehat{L}_j^a \widehat{H}_u^b - \mu \widehat{H}_d^a \widehat{H}_u^b \right] + M_{R_{ij}} \widehat{\nu}_i^c \widehat{X}_j + \frac{1}{2} \mu_{X_{ij}} \widehat{X}_i \widehat{X}_j, \end{aligned} \quad (2.1)$$

where $i, j = 1, 2, 3$ are generation indices. In the above, \widehat{H}_d and \widehat{H}_u are the down- and up-type Higgs superfields, \widehat{L}_i denotes the SU(2) doublet lepton superfields. The ‘‘Dirac’’-type right-handed neutrino mass term $M_{R_{ij}}$ conserves lepton number, while the ‘‘Majorana’’ mass term $\mu_{X_{ij}}$ violates it by two units. In view of this the total lepton number L is no longer conserved; notice however that in this formulation $(-1)^L$ remains a good quantum number. Since $M_{R_{ij}}$ conserves lepton number, in the limit $\mu_{X_{ij}} \rightarrow 0$, lepton number conservation can be restored. In this study we consider a general framework with three generations of $\widehat{\nu}^c$ and \widehat{X} ; we nevertheless recall that neutrino data can be successfully accommodated with only one generation of $\widehat{\nu}^c$ and \widehat{X} [17].

The soft SUSY breaking Lagrangian is given by

$$\begin{aligned} -\mathcal{L}_{\text{soft}} = & -\mathcal{L}_{\text{soft}}^{\text{MSSM}} + \widehat{\nu}_i^{c\dagger} m_{\widehat{\nu}_{ij}^c}^2 \widehat{\nu}_j^c + \widehat{X}_i^\dagger m_{\widehat{X}_{ij}}^2 \widehat{X}_j + (A_\nu^{ij} Y_\nu^{ij} \varepsilon_{ab} \widehat{\nu}_i^c \widehat{L}_j^a H_u^b + B_{M_R}^{ij} M_{R_{ij}} \widehat{\nu}_i^c \widehat{X}_j \\ & + \frac{1}{2} B_{\mu_X}^{ij} \mu_{X_{ij}} \widehat{X}_i \widehat{X}_j + \text{h.c.}), \end{aligned} \quad (2.2)$$

where $\mathcal{L}_{\text{soft}}^{\text{MSSM}}$ collects the soft SUSY breaking terms of the MSSM. $B_{M_R}^{ij}$ and $B_{\mu_X}^{ij}$ are the new parameters involving the scalar partners of the sterile neutrino states (notice that while the former conserves lepton number, the latter gives rise to a lepton number violating $\Delta L = 2$ term). Assuming a flavour-blind mechanism for SUSY breaking, we consider universal boundary conditions for the soft SUSY breaking parameters at some very high energy scale (e.g. the gauge coupling unification scale $\sim 10^{16}$ GeV),

$$m_\phi = m_0, M_{\text{gaugino}} = M_{1/2}, A_i = A_0 \mathbb{I}, B_{\mu_X} = B_{M_R} = B_0 \mathbb{I}. \quad (2.3)$$

¹We use the notation: $\widehat{\nu}^c = \widehat{\nu}_R^*$.

From Eq. (2.1) one can verify that the two singlets $\widehat{\nu}_i^c$ and \widehat{X}_i are differently treated in the superpotential, so that, while a $\Delta L = 2$ Majorana mass term is present for \widehat{X}_i ($\mu_{X_{ij}} \widehat{X}_i \widehat{X}_j$), no $\mu_{\nu_{ij}^c} \widehat{\nu}_i^c \widehat{\nu}_j^c$ term is included in \mathcal{W} . Although the latter term can indeed be present in a superpotential, where $(-1)^L$ is a good quantum number, we assume here for simplicity $\mu_{\nu_{ij}^c} = 0$. We notice that it is the magnitude of μ_X (and not that of μ_{ν^c}) which controls the size of the light neutrino mass [13,18], and that the absence of the mass term μ_{ν^c} does enhance the symmetry of the model (a non-vanishing, but small value of $\mu_{\nu_{ij}^c}$ does not have any effect on the qualitative features of the model). Here, μ_X will be considered as an effective parameter, no assumption being made on its origin. Such a parameter could be understood either dynamically or in a SUSY Grand Unified Theory framework [13,14,18,20]. Furthermore $\mu_{\nu^c} \ll \mu_X$ can also be realised in some extended frameworks [13].

2.1 Neutrino masses

We consider a general framework with three generations of sterile neutrinos ν_i^c and X_i . Consequently, one has the following symmetric (9×9) mass matrix \mathcal{M} in the basis $\{\nu, \nu^c, X\}$,

$$\mathcal{M} = \begin{pmatrix} 0 & m_D^T & 0 \\ m_D & 0 & M_R \\ 0 & M_R^T & \mu_X \end{pmatrix}, \quad (2.4)$$

Where, $m_D = \frac{1}{\sqrt{2}} Y_\nu v_u$ and M_R, μ_X are (3×3) matrices in family space. Assuming $m_D, \mu_X \ll M_R$, the diagonalization leads to an effective Majorana mass matrix for the light neutrinos [45],

$$m_\nu = m_D^T M_R^{T-1} \mu_X M_R^{-1} m_D = \frac{v_u^2}{2} Y_\nu^T (M_R^T)^{-1} \mu_X M_R^{-1} Y_\nu. \quad (2.5)$$

As mentioned earlier, one of the advantages of the inverse seesaw mechanism is that the smallness of the light neutrino masses is directly controlled by the size of μ_X . Hence the lepton number conserving mass parameters m_D and M_R can easily accommodate large (natural) Yukawa couplings ($Y_\nu \sim \mathcal{O}(1)$) and a right-handed neutrino mass scale around the TeV, see Eq. (2.5). In turn, this allows to have sizable contributions to cLFV observables, contrary to what occurs in the framework of, for example, a type-I seesaw.

In analogy to a type-I seesaw, one can define an effective right-handed neutrino mass term M such that

$$M^{-1} = (M_R^T)^{-1} \mu_X M_R^{-1}. \quad (2.6)$$

With this definition, the light neutrino mass matrix can be cast in a way strongly resembling a standard (type-I) seesaw equation

$$m_\nu = \frac{v_u^2}{2} Y_\nu^T M^{-1} Y_\nu. \quad (2.7)$$

This effective light neutrino mass matrix (m_ν) can be diagonalized as

$$U_{\text{PMNS}}^T m_\nu U_{\text{PMNS}} = \text{diag } m_i. \quad (2.8)$$

Using the above equations, one can express the neutrino Yukawa couplings ($Y_\nu = \frac{\sqrt{2}}{v_u} m_D$) as in [9] (in analogy to the Casas-Ibarra parameterization [46] in standard seesaw),

$$Y_\nu = \frac{\sqrt{2}}{v_u} \sqrt{\widehat{M}} R \sqrt{m_i} U_{\text{PMNS}}^\dagger, \quad (2.9)$$

where $\sqrt{\hat{M}}$ is the diagonal matrix² with the square roots of the eigenvalues of M and R is a 3×3 orthogonal matrix, parameterized by 3 complex angles, which encodes additional mixings. In our study of the different cLFV observables, we assume specific regimes for R .

Without loss of generality, we choose a basis where M_R is diagonal at the SUSY scale, i.e.,

$$M_{R_{ij}} = \text{diag } M_{R_{ii}}. \quad (2.10)$$

In addition, in the numerical evaluation, we shall also assume $\mu_{X_{ij}}$ to be diagonal, a simplifying assumption motivated by the fact that cLFV observables depend only indirectly on $\mu_{X_{ij}}$, as already discussed in the introduction. We will further explain this issue in Section 5.1. In the subsequent analysis, we assume M_R, μ_X to be free parameters, determined in order to comply with neutrino data.

Concerning neutrino oscillation data, there has been a very intense experimental activity related to the θ_{13} mixing angle, with very recent results from Double-Chooz [1], T2K [2], MINOS [3], Daya-Bay [4] and RENO [5]. We use in our analysis the (best-fit) results of [47], supplemented with the Daya-Bay measurement for θ_{13} [4]. Therefore, we consider the following set of parameters, namely the two mass-squared differences and the three mixing angles, given below with 3σ range [4, 47],

$$\begin{aligned} \sin^2 \theta_{12} &= 0.27 - 0.36, \\ \sin^2 \theta_{23} &= 0.39 - 0.64, \\ \sin^2 2\theta_{13} &= 0.092 \pm 0.06, \\ \Delta m_{21}^2 &= 7.09 - 8.19 \times 10^{-5} \text{ eV}^2, \\ |\Delta m_{31}^2| &= 2.18 - 2.73 \times 10^{-3} \text{ eV}^2. \end{aligned} \quad (2.11)$$

We also assume normal hierarchy ($\Delta m_{31}^2 > 0$). Updated global fits to all available experimental data have also appeared recently [6, 7]. However, these do not have a significant effect on our numerical results.

3 Z -boson mediated cLFV

In this section we shall discuss the enhancement of the Z -boson mediated contributions, presenting approximate results for the $Z - \ell_i - \ell_j$ effective vertex. We then proceed to discuss how, in different extensions of the MSSM, the Z -boson mediated contributions can significantly enhance several cLFV observables. The latter effect, which is absent in the MSSM, can have a strong impact on the theoretical predictions for cLFV rates, potentially leading to a very different phenomenology since $\text{Br}(\ell_i \rightarrow \ell_j \gamma)$ will no longer be the most constraining observables.

3.1 Enhancing cLFV with the Z -penguin

In the MSSM and in many of its extensions, photon penguins provide the dominant contributions to 3-body cLFV decays $\ell_i \rightarrow 3\ell_j$ [48, 49]. The only exception arises in the large $\tan \beta$ (and low m_A) regime, where large Higgs contributions are expected [50]³. However, it has recently been shown that many simple extensions of the (s)leptonic sector can lead to large enhancements of the

²In the subsequent sections we always consider scenarios where $M = \text{diag}(\hat{M}, \hat{M}, \hat{M})$. Therefore, for the sake of brevity, we use the simple notation M both for the matrix and its eigenvalues.

³A similar observation in the context of the inverse seesaw was recently made in [25].

Z -boson contributions [40], potentially leading to scenarios where the latter provide the dominant contribution to $\text{Br}(\ell_i \rightarrow 3\ell_j)$ ($> \text{Br}(\ell_i \rightarrow \ell_j \gamma)$). This can be understood from simple mass scaling considerations: let us consider the chargino-sneutrino 1-loop diagrams leading to $\ell_i \rightarrow 3\ell_j$. The photon-penguin contribution can be written as

$$A_a^{(c)L,R} = \frac{1}{16\pi^2 m_Z^2} \mathcal{O}_{A_a}^{L,R} s(x^2), \quad (3.1)$$

whereas the Z -contributions read

$$F_X = \frac{1}{16\pi^2 g^2 \sin^2 \theta_W m_Z^2} \mathcal{O}_{F_X}^{L,R} t(x^2), \quad (3.2)$$

with $X = \{LL, LR, RL, RR\}$. In the above $\mathcal{O}_y^{L,R}$ denote combinations of rotation matrices and coupling constants and $s(x^2)$ and $t(x^2)$ represent the Passarino-Veltman loop functions which depend on $x^2 = m_{\tilde{\chi}_-^2}^2/m_{\tilde{\nu}}^2$ (see [49]). Notice that the only mass scale involved in the A form factors is m_{SUSY} (the photon being massless). On the other hand, the mass scale in the F_X form factors is set, in this case, by the Z -boson mass (m_Z). Therefore, we conclude that $A \sim m_{\text{SUSY}}^{-2}$ and $F \sim m_Z^{-2}$. Since $m_Z^2 \ll m_{\text{SUSY}}^2$, the Z -penguin can, in principle, dominate over the photon penguin. Assuming that all loop functions, mixing matrices and coupling constants are of the same order, one can estimate

$$\frac{F}{A} \sim \frac{m_{\text{SUSY}}^2}{g^2 \sin^2 \theta_W m_Z^2} \sim 500 \quad \text{for} \quad m_{\text{SUSY}} = 300 \text{ GeV}. \quad (3.3)$$

Moreover, the $\ell_i \rightarrow 3\ell_j$ decay width depends on F^2 and A^2 , and thus the above ratio becomes even more pronounced⁴. However, a subtle cancellation between the different diagrams contributing to the leading Z -contribution [40] implies that in the MSSM, the photon penguin is found to be (numerically) dominant [48, 49]. To understand this, notice that the dominant contribution to $\ell_i \rightarrow 3\ell_j$ comes from diagrams where the leptons in the external legs are left-handed (the other cases are suppressed by the Yukawa couplings of the charged leptons). This is given by the form factor F_{LL} , usually written as

$$F_{LL} = \frac{F_L Z_L^{(l)}}{g^2 s_W^2 m_Z^2}, \quad (3.4)$$

where $Z_L^{(l)} = -\frac{g}{c_W}(-\frac{1}{2} + s_W^2)$ is the $Z - \ell_i - \ell_j$ tree-level coupling ($i = j$) and F_L is the $Z - \ell_i - \ell_j$ 1-loop effective vertex, with $i \neq j$, and with $c_W = \cos \theta_W$ and $s_W = \sin \theta_W$. F_L receives contributions from different 1-loop diagrams, and here we focus on the chargino-sneutrino loop contribution. Expanding in the chargino mixing angle, $\theta_{\tilde{\chi}^\pm}$, one can write (see Fig.1)

$$F_L = F_L^{(0)} + \frac{1}{2} \theta_{\tilde{\chi}^\pm}^2 F_L^{(2)} + \dots \quad (3.5)$$

Notice that there is no term in the expansion involving \tilde{H}^\pm at the leading order, nor at the 1st order, since there is no $\tilde{H}^\pm - \tilde{\nu}_L - \ell_L$ coupling. For this reason, only the wino contributes at the zeroth order in $\theta_{\tilde{\chi}^\pm}$. $F_L^{(0)}$ can be written as⁵

$$\left(F_L^{(0)}\right)_{ij} \equiv F_L^{(0)} = -\frac{1}{16\pi^2} \left(M_{\text{wave}}^{ij} + M_{\text{p1}}^{ij} + M_{\text{p2}}^{ij}\right), \quad (3.6)$$

⁴ From these considerations one can also conclude that in a very light SUSY scenario, with $m_{\text{SUSY}} \sim m_Z$, photon and Z -contributions to $\ell_i \rightarrow 3\ell_j$ are of the same order. This observation has been confirmed numerically, see section 5.2.

⁵ For the sake of clarity, we omit flavour indices in the expression for F_L (and in the expansion coefficients).

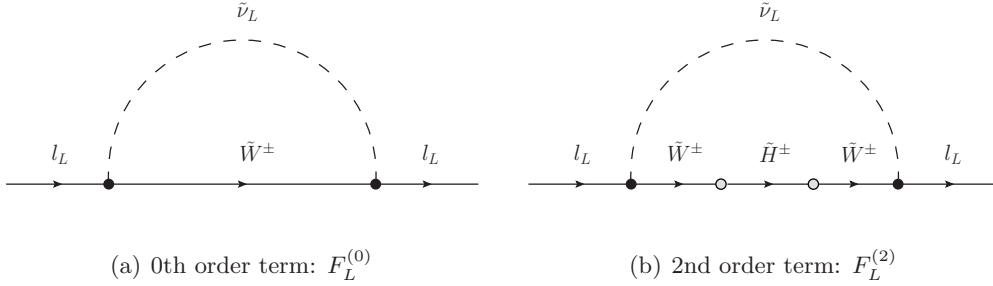


Figure 1: Diagrammatic representation of the F_L expansion in the chargino mixing angle, $\theta_{\tilde{\chi}^\pm}$.

with

$$M_{\text{wave}}^{ij} = -\frac{1}{2}g^2(g c_W - g' s_W)Z_V^{xi*}Z_V^{xj}f_{\text{wave}}^x, \quad (3.7)$$

$$M_{\text{p1}}^{ij} = g^3 c_W Z_V^{xi*}Z_V^{xj}f_{\text{p1}}^x, \quad (3.8)$$

$$M_{\text{p2}}^{ij} = -\frac{1}{2}g^2(g c_W + g' s_W)Z_V^{xi*}Z_V^{xj}f_{\text{p2}}^x, \quad (3.9)$$

where a sum over the index x is implicit. The terms in the sum come from different types of diagrams: wave function diagrams (M_{wave}) and penguins with the Z -boson attached to the chargino line (M_{p1}) or to the sneutrino line (M_{p2}). Moreover, Z_V is a 3×3 unitary matrix that diagonalizes the mass matrix of the sneutrinos. Here $f_{\text{wave}}^x = -B_1(m_{\tilde{\chi}_1^\pm}^2, m_{\tilde{\nu}_x}^2)$, $f_{\text{p1}}^x = \frac{1}{2}\tilde{C}_0(m_{\tilde{\nu}_x}^2, m_{\tilde{\chi}_1^\pm}^2, m_{\tilde{\chi}_1^\pm}^2) - m_{\tilde{\chi}_1^\pm}^2 C_0(m_{\tilde{\nu}_x}^2, m_{\tilde{\chi}_1^\pm}^2, m_{\tilde{\chi}_1^\pm}^2)$, $f_{\text{p2}}^x = \frac{1}{2}\tilde{C}_0(m_{\tilde{\chi}_1^\pm}^2, m_{\tilde{\nu}_x}^2, m_{\tilde{\nu}_x}^2)$; for the exact definitions of these loop functions, see [49]. The sum in Eq. (3.6) exactly vanishes, as can be verified by grouping the different terms

$$F_L^{(0)} = \frac{g^2}{32\pi^2} \left(g c_W Z_V^{xi*} Z_V^{xj} X_1^x + g' s_W Z_V^{xi*} Z_V^{xj} X_2^x \right) \quad (3.10)$$

with $X_1^x = f_{\text{wave}}^x - 2f_{\text{p1}}^x + f_{\text{p2}}^x$, $X_2^x = f_{\text{p2}}^x - f_{\text{wave}}^x$. Using the exact expressions for the loop functions [49], one finds that the masses cancel out and that these combinations become independent of $x = m_{\tilde{\chi}^-}/m_{\tilde{\nu}}$: $X_1^x = X_1 = -\frac{3}{4}$ and $X_2^x = X_2 = -\frac{1}{4}$, $\forall x$. Therefore, one is left with $F_L^{(0)} \propto \sum_x Z_V^{xi*} Z_V^{xj} = \left(Z_V^\dagger Z_V \right)^{ij}$, which vanishes for $i \neq j$ due to unitarity of the Z_V matrix⁶. In conclusion, the first non-vanishing term in the expansion appears at 2nd order in the chargino mixing angle, which naturally suppresses the Z -mediated contributions. This is the reason why the photon contributions turn out to be dominant in the MSSM.

However, there are many cases where the cancellation of the zeroth order term in the expansion no longer holds, as discussed in [40], where numerical examples were given, including the inverse SUSY seesaw. The introduction of new interactions for the (s)leptons, in particular, the one involving the Yukawa couplings Y_ν , modifies the previous conclusion for the MSSM: owing to the $\tilde{H}^\pm - \tilde{\nu}_R - \ell_L$ coupling, higgsino contributions for $F_L^{(0)}$ preclude the previously discussed cancellation. In fact, there is a non-zero $F_L^{(0)}$ contribution that enhances F_L by a huge factor leading to large Z -penguin mediated contributions to cLFV processes.

It is worth mentioning that the discussed cancellation only happens for wino diagrams and not for the higgsino ones. Therefore, F_R has already a finite zeroth order contribution in the MSSM. However, this is very small because of the tiny charged lepton Yukawa couplings.

⁶We notice that a similar behaviour was found in [51] in association to the $B \rightarrow X_s \ell^+ \ell^-$ decay.

Finally, although the previous discussion has been focused on $\ell_i \rightarrow 3\ell_j$, the same enhancement in the $Z - \ell_i - \ell_j$ effective vertex also affects other observables which are mediated by Z -boson exchange. This is the case for $\mu - e$ conversion in nuclei [39] and $\tau \rightarrow P^0\ell_i$, where P^0 is a pseudoscalar meson [52].

3.2 Approximate expression for the 1-loop $Z - \ell_i - \ell_j$ effective vertex

This section is devoted to deriving an analytical approximation for the 1-loop $Z - \ell_i - \ell_j$ effective vertex, $F_L \simeq F_L^{(0)}$, in the framework of the SUSY inverse seesaw.

Following the previous discussion, we will define this vertex with the lepton ℓ_i as incoming particle. The expression for $F_L^{(0)}$ obtained from the chargino-sneutrino loops⁷ can be decomposed as

$$F_L^{(0)} = -\frac{1}{16\pi^2} \left(F_{L,\text{wino}}^{(0)} + F_{L,\text{higgsino}}^{(0)} \right), \quad (3.11)$$

where $F_{L,\text{wino}}^{(0)}$ and $F_{L,\text{higgsino}}^{(0)}$ are the wino and higgsino contributions, respectively. The latter terms can be rewritten as

$$F_{L,\text{wino}}^{(0)} = -\frac{g^2}{2} Z_V^{xi*} Z_V^{xj} (g_{CW} Y_1^x + g' s_W Y_2^x) \quad (3.12)$$

$$F_{L,\text{higgsino}}^{(0)} = \frac{g}{4c_W} Y_\nu^{z'i*} Y_\nu^{zj} \left[\left(c_W^2 - \frac{1}{2} \right) \frac{1}{2} \delta_{zz'} - S_{xy} Z_V^{y,z'+3*} Z_V^{x,z+3} \tilde{C}_0(m_{\tilde{\chi}_2^\pm}^2, m_{\tilde{\nu}_x}^2, m_{\tilde{\nu}_y}^2) \right]. \quad (3.13)$$

where Z_V is now a 9×9 unitary matrix and sums over $x, y = 1, \dots, 9$ and $z, z' = 1, 2, 3$ are implicit. We have also defined the following combinations of loop functions:

$$Y_1^x = -\tilde{C}_0(m_{\tilde{\nu}_x}^2, m_{\tilde{\chi}_1^\pm}^2, m_{\tilde{\chi}_1^\pm}^2) + 2 C_0(m_{\tilde{\nu}_x}^2, m_{\tilde{\chi}_1^\pm}^2, m_{\tilde{\chi}_1^\pm}^2) - B_1(m_{\tilde{\chi}_1^\pm}^2, m_{\tilde{\nu}_x}^2) + \frac{1}{2} S_{xy} \tilde{C}_0(m_{\tilde{\chi}_1^\pm}^2, m_{\tilde{\nu}_x}^2, m_{\tilde{\nu}_y}^2) \quad (3.14)$$

$$Y_2^x = \frac{1}{2} S_{xy} \tilde{C}_0(m_{\tilde{\chi}_1^\pm}^2, m_{\tilde{\nu}_x}^2, m_{\tilde{\nu}_y}^2) + B_1(m_{\tilde{\chi}_1^\pm}^2, m_{\tilde{\nu}_x}^2) \quad (3.15)$$

and

$$S_{xy} = \sum_{k=1}^3 Z_V^{ky*} Z_V^{kx}. \quad (3.16)$$

Equations (3.12) and (3.13) are exact and do not involve any approximation nor assumption on the sneutrino mixing pattern. However, in order to render these expressions more transparent, let us now consider the following limit,

$$S_{xy} = \begin{cases} \delta_{xy} & \text{for } x, y \leq 3 \\ 0 & \text{for } x, y > 3 \end{cases} \quad (3.17)$$

This assumption actually corresponds to the MSSM, since in this case Z_V is a 3×3 unitary matrix. It also provides a very good approximation in the inverse seesaw when the Yukawa couplings are relatively small. In this framework⁸ the sneutrino mixing matrix Z_V , written in the

⁷The analogous neutralino-slepton loop diagrams provide extremely small contributions since they involve charged lepton Yukawa couplings and small mass insertions on the slepton propagators.

⁸As will be shown in our numerical analysis, regimes of small Yukawa couplings are actually favoured by current bounds on cLFV observables. For instance, $\mu - e$ conversion in gold leads to $(Y_\nu^\dagger Y_\nu)_{12} \lesssim 3 \times 10^{-4}$.

basis $\tilde{\nu}_x = (\tilde{\nu}_{1,2,3}, \tilde{\nu}_{1,2,3}^c, \tilde{X}_{1,2,3})$, is approximately given by

$$Z_V \simeq \left(\begin{array}{c|c} \mathbb{I}_3 & 0 \\ \hline 0 & Z_V^s \end{array} \right), \quad (3.18)$$

where \mathbb{I}_3 is the 3×3 identity matrix and Z_V^s is a 6×6 unitary matrix that diagonalizes the singlet sector. The negligible left-right mixing in the sneutrino sector thus justifies the approximation of Eq. (3.17).

In both cases, MSSM and the inverse seesaw with $\tilde{\nu}$ mixings as defined in Eq. (3.18), one can further simplify Eq. (3.12) by means of Eq. (3.17). It is straightforward to verify that Y_1^x reduces to $Y_1^x = X_1 = -\frac{3}{4}$, whereas Y_2^x reduces to $Y_2^x = X_2 = -\frac{1}{4}$. Therefore, using unitarity of the Z_V matrix, $Z_V^{xi*} Z_V^{xj} = \delta_{ij}$, the wino contribution simplifies to

$$F_{L,\text{wino}}^{(0)} = \frac{g^2}{8} \delta_{ij} (3g_{cW} + g'_{sW}) = \frac{g^3}{8c_W} \delta_{ij} (1 + 2c_W^2), \quad (3.19)$$

which vanishes in the case of flavour violating transitions ($i \neq j$). This is in perfect agreement with the Z -penguin cancellation in the MSSM, discussed in the previous subsection.

Let us now consider the higgsino contributions $F_{L,\text{higgsino}}^{(0)}$, not present in the MSSM. In this case, the results also simplify under the assumption of Eq. (3.18), which allows to cancel the last term in Eq. (3.13). Therefore, $F_{L,\text{higgsino}}^{(0)}$ can be written as

$$F_{L,\text{higgsino}}^{(0)} = \frac{g}{8c_W} \left(Y_\nu^\dagger Y_\nu \right)_{ij} \left(c_W^2 - \frac{1}{2} \right). \quad (3.20)$$

The above equation corresponds to the approximate LFV $Z - \ell_i - \ell_j$ 1-loop effective vertex.

We have explicitly checked that this formula does indeed reproduce the full numerical results to a very good approximation. Further refinements can be obtained by including other relevant (but sub-dominant) 1-loop diagrams. In particular, we found non-negligible sub-leading contributions arising from 1-loop diagrams involving charged Higgs and neutrinos. We also note that $F_L^{(1)}$ and the higher order terms in the expansion receive new contributions. However, the latter are (numerically) negligible when compared to $F_L^{(0)}$.

Finally, it is worth noticing that the $F_L^{(0)}$ effective vertex exhibits a crucial property: at leading order there is no dependence on any supersymmetric mass (however higher order terms in the expansion do indeed decrease for increasing SUSY masses).

There are well-known results in general quantum field theory (for both SUSY and non SUSY cases) regarding the decoupling theorem [53, 54], which seems not to apply in this case. Z -mediated processes exhibit a non-decoupling behaviour and large supersymmetric masses do not suppress the charged lepton flavour violating signatures induced by Z -boson exchange. This non-decoupling behaviour has also been found in flavour changing Higgs boson decays in the MSSM, both to hadronic [42, 43] and leptonic final states [44].

4 Lepton flavour violating observables

4.1 Current experimental situation and future prospects

The search for cLFV is a very active field with either dedicated experiments like MEG [55] or others with a broader program like B factories [56]. In this paper, we focus on leptonic observables, which

can be classified as radiative decays, e.g. $\mu \rightarrow e\gamma$, 3-body decays, e.g. $\tau \rightarrow 3\mu$, and neutrinoless conversion in muonic atoms, e.g. $\mu, \text{Ti} \rightarrow e, \text{Ti}$.

The experiments looking for radiative decays are quite different depending on the lepton in the initial state. If it is a muon, the only decay is $\mu \rightarrow e\gamma$ which is studied by dedicated experiments such as MEG [55]. This collaboration has plans for an upgrade that would improve the sensitivity to $\mathcal{O}(10^{-14})$. Radiative τ decays are studied at B factories, which are also τ factories, since the production cross-sections are very close at the $\Upsilon(4s)$ resonance. The current upper limits on $\text{Br}(\tau \rightarrow \mu\gamma)$ and $\text{Br}(\tau \rightarrow e\gamma)$ are given by the BaBar experiment, together with expected sensitivities at the future generation of B factories, e.g. Belle II and SuperB [56].

For the same reasons 3-body decays of the τ lepton are also usually searched for at B factories. The current upper limits come from the Belle experiment [57, 58] because of its larger data sample compared to BaBar. Since these observables are currently not limited by the background, significant improvements are expected at Belle II and SuperB [56]. The decay $\mu \rightarrow 3e$ has been investigated by the SINDRUM experiment [28] and, if approved, a future experiment named Mu3e at PSI could reach a sensitivity of 10^{-15} (after upgrades 10^{-16}) [59].

Neutrinoless conversion in muonic atoms has also been studied for different nuclei by the SINDRUM II collaboration [60, 61] which has set the current upper limits. In the future, the sensitivity is expected to be greatly improved by different projects⁹. For convenience, in our numerical study we will consider a future sensitivity in the range $10^{-16} - 10^{-18}$.

In addition to these low-energy observables, interesting phenomena are expected to be observed at colliders. One can have sizable widths for processes like $\chi_2^0 \rightarrow \chi_1^0 \ell_i^\pm \ell_j^\mp$, flavoured slepton mass splittings (especially between the first and second generation of left-handed sleptons) and finally the appearance of new edges in same-flavour dilepton mass distributions. Assuming a unique source of LFV (neutrino mass generation), the interplay of low- and high-energy LFV observables can strengthen or disfavour the underlying model of new physics. Illustrative examples of the potential of this interplay can be found for instance in [35–38].

4.2 $\mu - e$ conversion in nuclei

This process is particularly sensitive to the enhancement of the Z -penguin contribution. The conversion rate, relative to the muon capture rate, can be expressed as [39]

$$\begin{aligned} \text{CR}(\mu - e, \text{Nucleus}) &= \frac{p_e E_e m_\mu^3 G_F^2 \alpha^3 Z_{\text{eff}}^4 F_p^2}{8 \pi^2 Z} \\ &\times \left\{ \left| (Z + N) \left(g_{LV}^{(0)} + g_{LS}^{(0)} \right) + (Z - N) \left(g_{LV}^{(1)} + g_{LS}^{(1)} \right) \right|^2 + \right. \\ &\quad \left. \left| (Z + N) \left(g_{RV}^{(0)} + g_{RS}^{(0)} \right) + (Z - N) \left(g_{RV}^{(1)} + g_{RS}^{(1)} \right) \right|^2 \right\} \frac{1}{\Gamma_{\text{capt}}}. \quad (4.1) \end{aligned}$$

Z and N are the number of protons and neutrons in the nucleus and Z_{eff} is the effective atomic charge [67]. Similarly, F_p is the nuclear matrix element and Γ_{capt} represents the total muon capture rate. G_F is the Fermi constant, α is the fine structure constant, p_e and E_e ($\simeq m_\mu$ in the numerical evaluation) are the momentum and energy of the electron and m_μ is the muon mass.

⁹Mu2e [62, 63] is a future experiment at Fermilab with expected sensitivities of respectively 10^{-17} (phase I) and 10^{-18} (phase II with Project X). On the other hand, the first experiment that could be built at J-PARC is DeeMe [64] with an expected sensitivity of 2×10^{-14} in 2015. Then COMET [65] and PRISM/PRIME [66] would come with sensitivities of 10^{-15} (COMET Phase I, 2017), 10^{-17} (COMET phase II, 2021) and 10^{-18} (PRISM/PRIME) for a titanium nucleus.

In the above, $g_{XK}^{(0)}$ and $g_{XK}^{(1)}$ (with $X = L, R$ and $K = S, V$) represent the relevant isoscalar, and isovector couplings respectively, and are given by

$$\begin{aligned} g_{XK}^{(0)} &= \frac{1}{2} \sum_{q=u,d,s} \left(g_{XK(q)} G_K^{(q,p)} + g_{XK(q)} G_K^{(q,n)} \right), \\ g_{XK}^{(1)} &= \frac{1}{2} \sum_{q=u,d,s} \left(g_{XK(q)} G_K^{(q,p)} - g_{XK(q)} G_K^{(q,n)} \right). \end{aligned} \quad (4.2)$$

The numerical values of G_K can be found in [39].

Similar to other observables involving four fermions, the $\mu - e$ conversion rate receives contributions from γ -, Z - and Higgs-penguins as well as box diagrams. The corresponding couplings are,

$$\begin{aligned} g_{LV(q)} &= g_{LV(q)}^\gamma + g_{LV(q)}^Z + g_{LV(q)}^B, \\ g_{LS(q)} &= g_{LS(q)}^H + g_{LV(q)}^B \end{aligned} \quad (4.3)$$

where $g_{LX(q)}^\gamma$, $g_{LX(q)}^Z$, $g_{LS(q)}^H$, $g_{LX(q)}^B$ (with $X = V, S$) represent the couplings of the photon, Z , H and box diagrams, respectively. Again, considering that the Z -boson is at the origin of the dominant contribution¹⁰, we focus on $g_{LV(q)}^Z$. We thus have

$$g_{LV(q)} \equiv g_{LV(q)}^Z = -\frac{\sqrt{2}}{G_F} \frac{Z_L^q + Z_R^q}{2} \frac{F_L}{m_Z^2} \quad (4.4)$$

$$\equiv \bar{g}(q) \frac{F_L}{m_Z^2}, \quad (4.5)$$

and $g_{RV(q)} = g_{LV(q)}|_{L \leftrightarrow R}$. The $Z - \bar{q} - q$ couplings (Z_L^q, Z_R^q) can be written as

$$Z_L^{(q)} = -\frac{g}{c_W} [T_3^q - Q_q s_W^2], \quad (4.6)$$

$$Z_R^{(q)} = \frac{g}{c_W} Q_q s_W^2, \quad (4.7)$$

with $s_W = \sin \theta_W$ and $c_W = \cos \theta_W$. Then, considering that $F_R \ll F_L$, we have

$$\begin{aligned} \text{CR}(\mu - e, \text{Nucleus}) &= \frac{p_e E_e m_\mu^3 G_F^2 \alpha^3 Z_{\text{eff}}^4 F_p^2}{8 \pi^2 Z} \times \left| (Z + N) g_{LV}^{(0)} + (Z - N) g_{LV}^{(1)} \right|^2 \frac{1}{\Gamma_{\text{capt}}} \\ &= \frac{p_e E_e m_\mu^3 G_F^2 \alpha^3 Z_{\text{eff}}^4 F_p^2}{8 \pi^2 Z} \times \left| (Z + N) \bar{g}_{LV}^{(0)} + (Z - N) \bar{g}_{LV}^{(1)} \right|^2 \frac{F_L^2}{m_Z^4} \frac{1}{\Gamma_{\text{capt}}}, \end{aligned} \quad (4.8)$$

where

$$\bar{g}_{LV}^{(0,1)} = \frac{1}{2} \sum_{q=u,d,s} \bar{g}(q) \left(G_V^{(q,p)} \pm G_V^{(q,n)} \right).$$

Finally, substituting F_L and denoting the hadronic coefficient $\left| (Z + N) \bar{g}_{LV}^{(0)} + (Z - N) \bar{g}_{LV}^{(1)} \right|^2 = C_{\text{Had}}$, we have

$$\text{CR}(\mu - e, \text{Nucleus}) = \frac{p_e E_e m_\mu^3 G_F^2 \alpha^3 Z_{\text{eff}}^4 F_p^2 g^2}{2^{17} \pi^4 Z c_W^2} \times C_{\text{Had}} \frac{(c_W^2 - \frac{1}{2})^2}{m_Z^4} \left(Y_\nu^\dagger Y_\nu \right)_{12} \frac{1}{\Gamma_{\text{capt}}}. \quad (4.9)$$

This approximate formula is valid for scenarios where Z -boson provides the dominant contribution to the conversion rate.

¹⁰We stress that in our numerical analysis, we will take into account all contributions to the CR. We refer the reader to [39] for the corresponding formulae.

4.3 $\text{Br}(\ell_i \rightarrow 3\ell_j)$

As we discussed in Section 3, the Z -penguin can provide the dominant contribution to the decay width of $\ell_i \rightarrow 3\ell_j$ in the inverse seesaw extension of MSSM. In the limit of Z -penguin dominance, the decay width can be cast as [48, 49]

$$\begin{aligned}\Gamma(\ell_i \rightarrow 3\ell_j) &\simeq \frac{e^4}{512\pi^3} m_{\ell_i}^5 \frac{2}{3} (F_{LL}^2 + F_{RR}^2 + F_{LR}^2 + F_{RL}^2) \\ &\simeq \frac{e^4}{512\pi^3} m_{\ell_i}^5 \frac{2}{3} F_{LL}^2.\end{aligned}\quad (4.10)$$

The complete expression for F_{LL} can be derived using Eqs. (3.4),(3.11),(3.19) and (3.20),

$$F_{LL} = -\frac{(\frac{1}{2} - s_W^2)}{128\pi^2 s_W^2 c_W^2 m_Z^2} \left[g^2 \delta_{ij} (1 + 2c_W^2) + (Y_\nu^\dagger Y_\nu)_{ij} \left(c_W^2 - \frac{1}{2} \right) \right] \quad (4.11)$$

$$= -\frac{(\frac{1}{2} - s_W^2)^2}{128\pi^2 s_W^2 c_W^2 m_Z^2} (Y_\nu^\dagger Y_\nu)_{ij} \quad (i \neq j), \quad (4.12)$$

so that the decay width for $\Gamma(\ell_i \rightarrow 3\ell_j)$ is given by

$$\Gamma(\ell_i \rightarrow 3\ell_j) = \frac{e^4 (\frac{1}{2} - s_W^2)^4}{3 \cdot 2^{22} \pi^7 s_W^4 c_W^4 m_Z^4} m_{\ell_i}^5 (Y_\nu^\dagger Y_\nu)_{ij}^2. \quad (4.13)$$

In this limit one recovers a correlation between $\text{CR}(\mu - e, \text{Nucleus})$ and $\text{Br}(\mu \rightarrow 3e)$, which we shall briefly mention in our numerical results.

4.4 $\text{Br}(\tau \rightarrow P^0 \ell_i)$

τ decays into a light charged lepton and a pseudoscalar meson¹¹, $P^0 = \pi^0, \eta, \eta'$, can also be significantly enhanced in this framework, owing to Z -boson mediation. The corresponding branching ratio can be written as [52]

$$\text{Br}(\tau \rightarrow P^0 \ell_i) = \frac{1}{4\pi} \frac{\lambda^{1/2}(m_\tau^2, m_{\ell_i}^2, m_P^2)}{m_\tau^2 \Gamma_\tau} \frac{1}{2} \sum |T|^2, \quad (4.14)$$

where $\lambda(x, y, z) = (x + y - z)^2 - 4xy$ and Γ_τ is the total decay width of the τ lepton. The averaged squared amplitude summed over initial and final states is given by

$$\frac{1}{2} \sum |T|^2 = \frac{1}{4m_\tau} \sum_{k,m} \left[2m_{\ell_i} m_\tau (a_P^k a_P^{m*} - b_P^k b_P^{m*}) + (m_\tau^2 + m_{\ell_i}^2 - m_P^2) (a_P^k a_P^{m*} + b_P^k b_P^{m*}) \right], \quad (4.15)$$

with $k, m = Z, A^0$. Focusing on the Z -boson contributions, we have

$$\begin{aligned}a_P^Z &= -\frac{g}{2 \cos \theta_W} \frac{F_\pi C(P)}{2 m_Z^2} (m_\tau - m_{\ell_i}) (F_L + F_R), \\ b_P^Z &= \frac{g}{2 \cos \theta_W} \frac{F_\pi C(P)}{2 m_Z^2} (m_\tau + m_{\ell_i}) (F_R - F_L),\end{aligned}\quad (4.16)$$

¹¹We do not consider final states with a K^0 as this would involve additional suppression due to the double penguin.

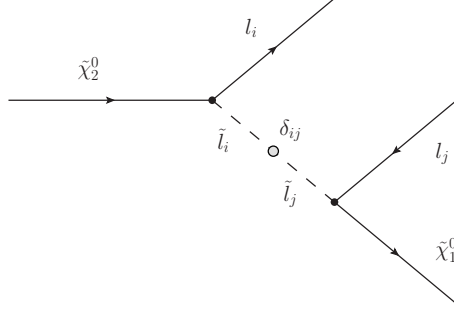


Figure 2: Feynman diagram contributing to $\text{Br}(\tilde{\chi}_2^0 \rightarrow \tilde{\chi}_1^0 \ell_i \ell_j)$. The white circle represents a LFV mass insertion in the charged slepton propagator.

where, $F_R = F_L|_{L \leftrightarrow R}$, which is in general small. In the above, $F_\pi \simeq 92.4$ MeV is the pion decay constant while the functions $C(P)$ have been defined in [52]. In the limit $F_R \ll F_L$, we have

$$\frac{1}{2} \sum |T|^2 = \frac{1}{256 m_\tau} \frac{g^2 F_\pi^2 C(P)^2}{c_W^2 m_Z^4} [-8m_\tau^2 m_{\ell_i}^2 + (m_\tau^2 + m_{\ell_i}^2 - m_P^2)(m_\tau^2 + m_{\ell_i}^2)] F_L^2. \quad (4.17)$$

Finally, using the expression for F_L , one finds

$$\begin{aligned} \frac{1}{2} \sum |T|^2 &= \frac{1}{2^{19} m_\tau} \frac{g^4 F_\pi^2 C(P)^2}{\pi^4 c_W^4 m_Z^4} [-8m_\tau^2 m_{\ell_i}^2 + (m_\tau^2 + m_{\ell_i}^2 - m_P^2)(m_\tau^2 + m_{\ell_i}^2)] \\ &\quad \times (c_W^2 - \frac{1}{2})^2 (Y_\nu^\dagger Y_\nu)_{i3}^2. \end{aligned} \quad (4.18)$$

Although this approximate formula corresponds to leading order estimates, in the numerical evaluation, we take into account all contributions from the Z - and Higgs bosons.

4.5 $\text{Br}(\ell_i \rightarrow \ell_j \gamma)$

For completeness, we discuss the radiative decays $\ell_i \rightarrow \ell_j \gamma$. These observables, which have been studied in great detail in [9, 48, 68], are not sensitive to the Z -mediation. It is however known that, for small values of M_R , the branching fraction can easily reach the experimental sensitivity, even in the absence of supersymmetric contributions [9]. In the following section, considering both heavy singlet neutrino as well as supersymmetric contributions, we will explore the part of the parameter space where $\text{Br}(\ell_i \rightarrow \ell_j \gamma)$ is within experimental sensitivity reach.

4.6 Collider observables: $\text{Br}(\tilde{\chi}_2^0 \rightarrow \tilde{\chi}_1^0 \ell_i \ell_j)$ and $\Delta m_{\tilde{\ell}}$

So far, we have only addressed low-energy observables. However, cLFV collider observables such as $\text{Br}(\tilde{\chi}_2^0 \rightarrow \tilde{\chi}_1^0 \ell_i \ell_j)$ and the slepton mass splittings $\Delta m_{\tilde{\ell}} (m_{\tilde{\ell}_i} - m_{\tilde{\ell}_j})$ are also relevant in scenarios that provide a strong connection between low- and high-energy lepton flavour violation [35–38].

However, in the model under investigation, one expects that these high-energy observables will be of little relevance when compared to the low-energy cLFV observables. For example, the decay $\tilde{\chi}_2^0 \rightarrow \tilde{\chi}_1^0 \ell_i \ell_j$ is induced by diagrams like the one shown in Figure 2. As we will verify in the following section, the experimental limits on the low-energy observables require small neutrino Yukawa couplings (typically of order $\sim 10^{-3} - 10^{-2}$), which in turn leads to low $\tilde{\chi}_2^0 \rightarrow \tilde{\chi}_1^0 \ell_i \ell_j$ rates and small mass splittings.

For completeness, we have also studied LFV decays such, as $Z \rightarrow \ell_i \ell_j$ and $h^0 \rightarrow \ell_i \ell_j$. However, as explained below, no enhancement was found.

5 Numerical results

In this section we present our numerical results. We begin by introducing the basic setup for our computation and show some results concerning the relative importance of the different contributions to the cLFV observables. We then discuss our results for the rates of cLFV observables, emphasising the most relevant features of this model. Finally, we provide a brief summary of the main results, which we illustrate via some representative benchmark points.

5.1 Setup

Our numerical results have been obtained with a `SPheno` [69, 70] code generated with the Mathematica package `SARAH` [71–73]. The computation of the LFV observables is based on the results presented in [39, 49, 52], which we extended to the inverse seesaw case.

In what concerns the supersymmetric parameters, the model is characterised by

$$m_0, M_{1/2}, A_0, \tan \beta, \text{sign}(\mu), B_0. \quad (5.1)$$

Due to their little influence on the relevant observables, we fix $\text{sign}(\mu)$ (+) and $B_0 (= 0)$ in our scans¹². We have explicitly checked that only $\mu \rightarrow e\gamma$ depends on the B_0 parameter. This can be understood from its effect on the sneutrino spectrum, which in turn strongly affects $\text{Br}(\mu \rightarrow e\gamma)$. We find that in some cases one can enhance $\text{Br}(\mu \rightarrow e\gamma)$ by as much as one order of magnitude if one uses B_0 to fine-tune the superparticle masses. The other observables are nearly independent of B_0 .

Concerning the remaining cMSSM-like parameters, m_0 , $M_{1/2}$, A_0 and $\tan \beta$, we will consider some specific scenarios. We nevertheless recall that the Z -penguin, dominant in most of the parameter space, has a very mild dependence on the cMSSM parameters, so that our conclusions for the Z -boson mediated processes are quite general. On the other hand, for the radiative $\ell_i \rightarrow \ell_j \gamma$, the dependence on the SUSY parameters cannot be neglected. These observables have been studied in SUSY and non-SUSY scenarios [9, 17, 74, 75] and we include them in our analysis for completeness. As we will see, only for very low values of M_R or when the superparticles in the loop are light, they become the most constraining observables.

As explained in Section 2.1, we will work in the basis where M_R is a diagonal matrix and compute the resulting Yukawa couplings by means of the Casas-Ibarra parameterisation [46]. In this basis, both Y_ν and μ_X can be in general non-diagonal. In fact, neutrino mixing requires off-diagonal entries in at least one of these two matrices. In principle, one can consider two limits: (1) Y_ν *limit*: Y_ν contains off-diagonal entries and μ_X is diagonal, and (2) μ_X *limit*: Y_ν is diagonal and μ_X contains off-diagonal entries (any phenomenologically allowed scenario will be either Y_ν limit, μ_X limit or an intermediate case). However, the off-diagonal elements in μ_X have no impact on the phenomenology in the charged lepton sector, since this parameter does not appear in the coefficients of the operators relevant for the cLFV transitions. Therefore, in the μ_X limit (where Y_ν is diagonal), all cLFV observables vanish. Thus, we choose to work in the Y_ν limit, assuming $\mu_X = \hat{\mu}_X \mathbb{I}$, where \mathbb{I} is the 3×3 identity matrix, which in turn maximises the lepton flavour violating effects allowed by this model. However, we stress that the model cannot be ruled out by the non-observation of cLFV processes, since one can always approach the μ_X limit to suppress the corresponding cLFV observables.

Concerning the M_R matrix, we will consider two scenarios: degenerate and non-degenerate spectrum, for simplicity presenting our results for the first one. In any case, and as shown

¹²It is worth recalling that B_0 only affects the sneutrino sector. μ and B_μ are computed using the tadpole equations at the SUSY scale.

below, the Z -boson mediated processes have very little dependence on the right-handed (s)neutrino spectrum. We further choose $R = 1$ (see Eq. (2.9)) in order to keep the discussion as simple as possible¹³.

Let us now discuss the relevant parameters for the cLFV observables. As explained above, μ_X has very little impact on the phenomenology, since it only affects LFV due to its relation to the size of Y_ν . On the other hand, M_R has a stronger impact, since it affects the masses of the singlet states, but, as already explained, the Z -penguins are only slightly sensitive to the spectrum. Therefore, the impact of M_R on cLFV is rather small, only via the size of the Yukawa couplings. The relevant quantities for the analysis are $M \sim \frac{M_R^2}{\mu_X}$ (as defined in Eq. (2.6)), controlling the size of the Yukawa couplings Y_ν , and M_R , which plays a sub-dominant rôle¹⁴. Therefore, we will study the variation of the cLFV rates with respect to M , showing how different possibilities for M_R affect the numerical results.

In this work, we do not take into account the LHC Higgs mass constraint on the allowed parameter space. Our conclusions for lepton flavour violating observables are expected to hold when the Higgs mass constraint is forced upon the cMSSM parameter space. Indeed, one can always find regions in the cMSSM parameter space that fulfill the recent results from the LHC [76, 77] and Tevatron [78], pointing towards a Higgs mass in the 125 GeV range: this can be achieved with large A_0 (to increase the mixing in the stop sector) and a moderately large $\tan \beta$, see for example [79–81]. This conclusion can easily be generalized to the supersymmetric inverse seesaw.

In the limit of small Yukawa couplings, the singlet sector contributions to the Higgs mass are negligible [82]. In fact, and as we will see below, limits on cLFV processes set important constraints on the Yukawa couplings, forcing them to be below $Y_\nu \sim 10^{-3} - 10^{-2}$ (unless one is working in the μ_X limit defined above). Thus one simply recovers the cMSSM result. We will discuss a particular benchmark point where this is explicitly shown.

5.2 Relative importance of the different contributions

We start this section by considering the different contributions of the SM/SUSY particles to the cLFV observables. We display our results for $\ell_i \rightarrow 3\ell_j$ and $\mu - e$ conversion in gold, although the conclusions drawn here can be easily extended to other cLFV observables.

Figure 3 shows how the different relative contributions to $\text{Br}(\mu \rightarrow 3e)$ and $\mu - e$ conversion in $^{197}_{79}\text{Au}$ depend on the SUSY scale, setting for simplicity $m_0 = M_{1/2}$. The relative contributions, denoted as c_i , are defined as

$$c_i = \frac{|R_i|}{\sqrt{\sum_k R_k^2}}, \quad (5.2)$$

where R_i is the rate (branching ratio in case of $\mu \rightarrow 3e$ and conversion rate in case of $\mu - e$ conversion in Au) that would be obtained should the i -contribution to the process be the only one. These numerical results have been obtained with fixed values for $A_0 = -300$ GeV, $B_0 = 0$, $\tan \beta = 10$ and $\text{sign}(\mu) = +$. Nevertheless, we have verified that a different set of parameters would lead to similar results.

For $\text{Br}(\mu \rightarrow 3e)$ the different contributions include (γ , Z , h , interference $\gamma - Z$, interference $\gamma - h$, interference $Z - h$). Note that h includes both Higgs and box contributions, grouped together

¹³In general, the limit $R = 1$ translates into a “conservative” limit for flavour violation: apart from possible cancellations, and for a fixed seesaw scale, this limit typically provides a lower bound on the generated cLFV rates.

¹⁴The exception to this rule is $\mu \rightarrow e\gamma$: as one lowers M_R , one enhances $\text{Br}(\mu \rightarrow e\gamma)$; this is due to non-SUSY contributions, see Section 4.5. Such an effect is less pronounced in other observables.

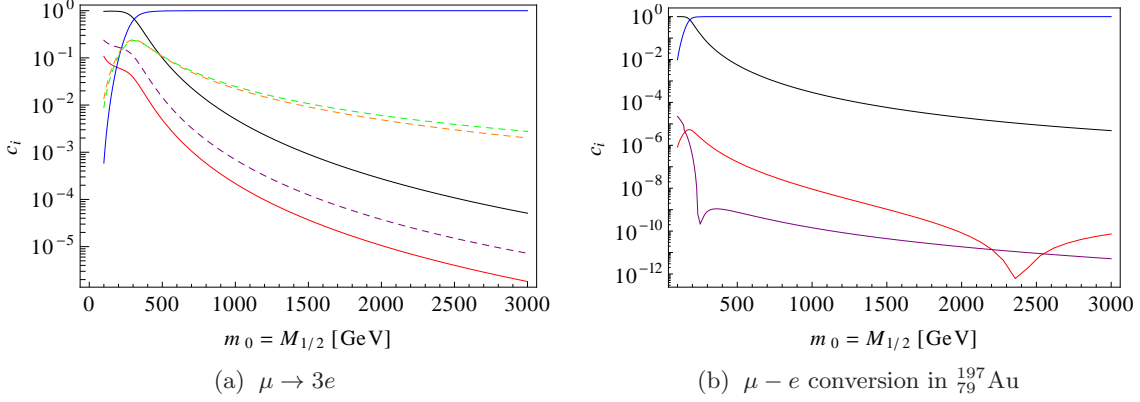


Figure 3: Relative contributions to $\text{Br}(\mu \rightarrow 3e)$ (left-hand side) and $\mu - e$ conversion in $^{197}_{79}\text{Au}$ (right-hand side) as a function of $m_0 = M_{1/2}$ for a degenerate singlet spectrum with $\hat{M}_R = 10$ TeV and $M = 10^{11}$ GeV. The rest of the cMSSM parameters are set to $A_0 = -300$ GeV, $B_0 = 0$, $\tan\beta = 10$ and $\text{sign}(\mu) = +$. On the left-hand side, solid lines represent individual contributions, γ (black), Z (blue) and h (red) whereas the dashed lines represent interference terms, $\gamma - Z$ (green), $\gamma - h$ (purple) and $Z - h$ (orange). Note that in this case h includes both Higgs and box contributions. On the right-hand side interference terms are not shown to make the results clearer. The individual contributions are γ (black), Z (blue) and h (red) and boxes (purple).

in [49]. Figure 3(a) clearly shows that the Z -boson contribution to the process is the dominant one. Only for very low $m_0 = M_{1/2}$ can one find competitive (even dominant) photon contributions, as expected from the theoretical arguments, see Section 3. However, the low m_0 region has already been excluded by direct collider searches [83, 84].

A very similar behaviour is found for $\mu - e$ conversion in Au, where the Z -boson contribution turns out to be the dominant one as well. Figure 3(b) depicts the different individual contributions to the conversion rate, with $i = (\gamma, Z, h, \text{boxes})$. In this case, interference terms have not been shown to simplify the plot and to render the main results more visible. Again, as occurred for $\text{Br}(\mu \rightarrow 3e)$, the photon contribution becomes important for light SUSY scenarios (lower values of $m_0 = M_{1/2}$). The little dip in the boxes curve is due to small numerical instabilities in the loop function computation. The reduction of the photon contribution in $\mu - e$ conversion, when compared to the $\text{Br}(\mu \rightarrow 3e)$, is due to the smaller electric charges of the quarks compared to those of the leptons.

Finally, we show in Figure 4 the absolute individual contributions to $\text{Br}(\mu \rightarrow 3e)$ as a function of $m_0 = M_{1/2}$. This plot, complementary to the one on the left-hand side of Figure 3, serves to illustrate the non-decoupling behaviour of the Z -boson contributions. As one increases $m_0 = M_{1/2}$, the resulting SUSY spectrum becomes heavier and the photon, Higgs and box contributions to $\text{Br}(\mu \rightarrow 3e)$ clearly decrease. In contrast, the Z -penguin contribution remains constant in the heavy SUSY limit, in which case the 1-loop effective $Z - \mu - e$ coupling can be well described by the leading order term $F_L^{(0)}$, see Eq. (3.20).

In conclusion, in the framework of the inverse seesaw, should the Z -penguin be present, it will provide the dominant contribution to cLFV observables (except in the case of a very light SUSY spectrum). This result clearly justifies the approximations of Section 4.

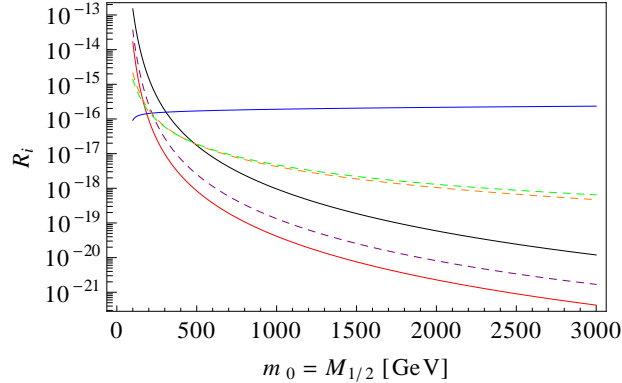


Figure 4: Absolute contributions to $\text{Br}(\mu \rightarrow 3e)$ as a function of $m_0 = M_{1/2}$. The parameters and the color code are the same as in figure 3.

5.3 $\mu - e$ conversion in nuclei

After the discussion on the relative size of the different individual contributions, we proceed to study the different cLFV observables and begin with $\mu - e$ conversion rates in nuclei¹⁵.

We first address the degenerate singlet scenario, $M_R = \text{diag}(\hat{M}_R, \hat{M}_R, \hat{M}_R)$. The more general case of a hierarchical spectrum will be briefly discussed in Section 5.7, although we should mention that the difference for this observable is small and does not affect our conclusions.

Figure 5 shows the $\mu - e$ conversion rates for different nuclei $^{197}_{79}\text{Au}$ (left) and $^{48}_{22}\text{Ti}$ (right), as a function of M for three different \hat{M}_R values (100 GeV, 1 TeV, 10 TeV). Again, we take $A_0 = -300$ GeV, $\tan\beta = 10$, $\text{sign}(\mu) = +$ and $B_0 = 0$, but m_0 and $M_{1/2}$ are randomly taken in the range $[0, 3$ TeV]. Note that there is a sharp correlation with M , hardly distorted by the changes in m_0 and $M_{1/2}$. For the red and black dots, this is a consequence of Z -boson dominance, as discussed in Section 3. The blue dots correspond to the limiting case of non-SUSY photon-penguin dominance (associated to $\hat{M}_R = 100$ GeV), which leads to larger values for $\mu - e$ conversion rates.

	M [GeV]	$(Y_\nu^\dagger Y_\nu)_{12}$
CR _{Au} (current)	10^{12}	2.7×10^{-4}
CR _{Ti} (current)	4×10^{12}	10^{-3}
CR _{Ti} (future: 10^{-16})	2×10^{10}	5.5×10^{-6}
CR _{Ti} (future: 10^{-18})	2×10^9	5.5×10^{-7}

Table 1: Approximate limits on M and $(Y_\nu^\dagger Y_\nu)_{12}$ from the non-observation of $\mu - e$ conversion in nuclei. This table includes current experimental bounds and future expected sensitivities [62, 63, 65].

The non-observation of $\mu - e$ conversion in gold, $^{197}_{79}\text{Au}$, sets an upper bound on the size of M , $M \sim 10^{12}$ GeV (the exact value slightly dependent on \hat{M}_R).

Conservative limits will be derived from the results obtained for $\hat{M}_R \gtrsim 1$ TeV. We stress that lower values for \hat{M}_R would lead to more stringent limits. This approximate limit on M can be translated into constraints for $(Y_\nu^\dagger Y_\nu)_{12}$, the flavour violating combination of Yukawa couplings controlling $\mu - e$ transitions. Using Eqs. (2.6) and (2.9), we find that this limit is 2.7×10^{-4} . On the other hand, $\mu - e$ conversion in $^{48}_{22}\text{Ti}$ has a slightly more relaxed experimental bound, which in

¹⁵This has been studied in [10] for the non-supersymmetric inverse seesaw case.

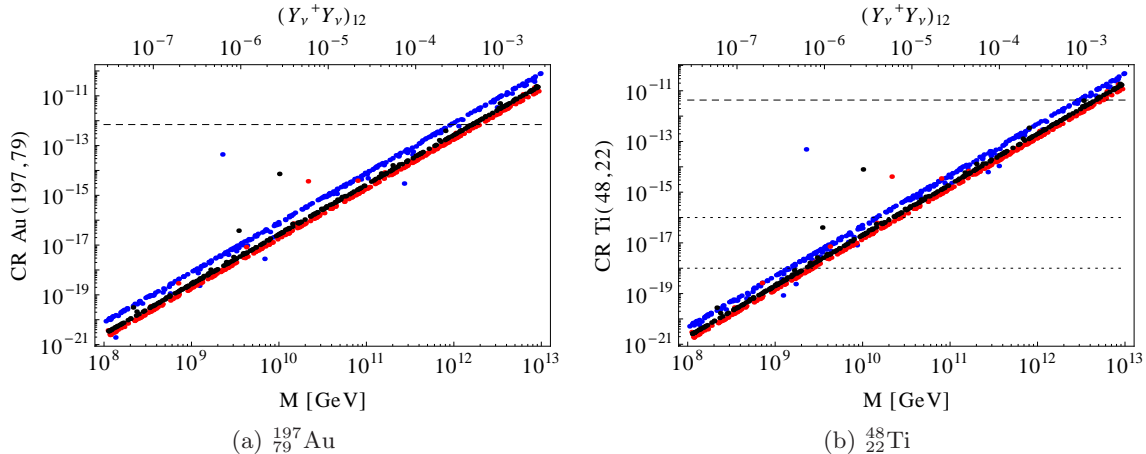


Figure 5: $\mu - e$ conversion rates in $^{197}_{79}\text{Au}$ (left) and $^{48}_{22}\text{Ti}$ (right), as a function of M and $(Y_\nu^\dagger Y_\nu)_{12}$ for different \hat{M}_R values: $\hat{M}_R = 100$ GeV (blue), $\hat{M}_R = 1$ TeV (red) and $\hat{M}_R = 10$ TeV (black). We set $A_0 = -300$ GeV, $\tan\beta = 10$, $\text{sign}(\mu) = +$ and $B_0 = 0$, and we randomly vary m_0 and $M_{1/2}$ in the range $[0, 3]$ TeV]. The horizontal dashed lines represent the current experimental bounds and the dotted ones represent the expected future sensitivities.

turn implies less stringent limits on both M and $(Y_\nu^\dagger Y_\nu)_{12}$, 4×10^{12} GeV and 10^{-3} , respectively. However, there are plans to improve the experimental sensitivities for $\mu - e$ conversion in titanium with expected sensitivities in the $10^{-18} - 10^{-16}$ range [62, 63, 65]. Should this be the case, and no $\mu - e$ conversion events be observed, the limits on the parameters of the inverse seesaw model would be greatly improved.

In Table 1 we compute approximate limits for M and $(Y_\nu^\dagger Y_\nu)_{12}$, as obtained from current experimental bounds and future expected sensitivities. Such a (rough) estimate is possible due to the little dependence of this result on \hat{M}_R and on the cMSSM parameters, as shown in Figure 5. However, from these estimates, we can safely conclude that $\mathcal{O}(1)$ Yukawa couplings, as typically chosen in the literature, are clearly ruled out since they would induce excessively large cLFV effects. This would imply that $(Y_\nu^\dagger Y_\nu)_{12} \sim 1$, corresponding to $M \sim 10^{14}$ GeV, clearly out of the allowed range¹⁶.

5.4 $\ell_i \rightarrow 3\ell_j$

Concerning the 3-body decays $\ell_i \rightarrow 3\ell_j$ we focus on $\mu \rightarrow 3e$, due to its very challenging experimental bound. Since the Z -boson does not differentiate between leptonic flavours, the same behaviour and enhancement can be found for the cLFV τ 3-body decays into leptons.

As discussed in [40], the branching ratio for $\mu \rightarrow 3e$ is greatly enhanced by the Z -penguin. In fact, it turns out that this process is only *slightly* less constraining than $\mu - e$ conversion in nuclei. In Figure 6, the $\text{Br}(\mu \rightarrow 3e)$ is depicted as a function of M , and for three representative \hat{M}_R values, again assuming a degenerate singlet spectrum. As was the case of $\mu - e$ conversion in nuclei, the dependence on the cMSSM parameters is essentially negligible. Similarly, the scenario with $\hat{M}_R = 100$ GeV is dominated by the non-supersymmetric photonic penguins and larger branching

¹⁶This statement only applies to off-diagonal Yukawa couplings. As explained at the beginning of this section, the μ_X limit, in which the Y_ν matrices are exactly diagonal, suppresses all cLFV observables and thus $\mathcal{O}(1)$ diagonal Yukawa couplings would be allowed.

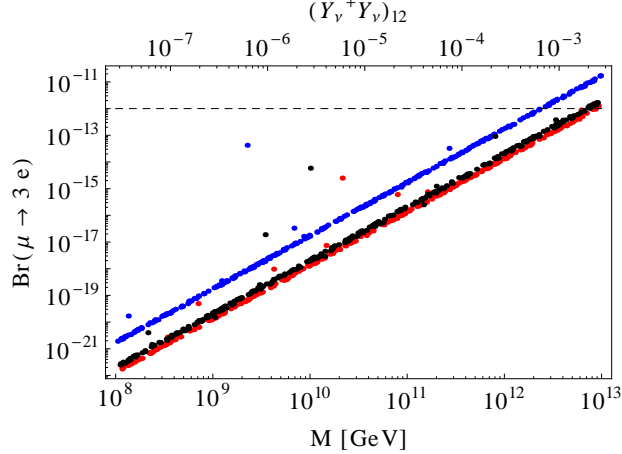


Figure 6: $\text{Br}(\mu \rightarrow 3e)$ as a function of M and $(Y_\nu^\dagger Y_\nu)_{12}$ for different \hat{M}_R values: $\hat{M}_R = 100$ GeV (blue), $\hat{M}_R = 1$ TeV (red) and $\hat{M}_R = 10$ TeV (black). The cMSSM parameters are taken as in figure 5. The horizontal dashed line represents the current experimental bound.

ratios can thus be obtained. As can be seen, the corresponding limits on M and $(Y_\nu^\dagger Y_\nu)_{12}$ would be slightly more relaxed than those arising from $\mu - e$ conversion in gold and titanium.

It is straightforward to obtain the following relation between the branching ratios of different $\ell_i \rightarrow 3\ell_j$ channels

$$\frac{\text{Br}(\ell_i \rightarrow 3\ell_j)}{\text{Br}(\ell_m \rightarrow 3\ell_n)} = \frac{(Y_\nu^\dagger Y_\nu)_{ij}^2}{(Y_\nu^\dagger Y_\nu)_{mn}^2} \frac{m_{\ell_i}^5 \tau_i}{m_{\ell_m}^5 \tau_m}, \quad (5.3)$$

where $\tau_{i,m}$ are the life-times of the leptons. Equation (5.3) provides a very good approximation to the numerical results and allows to conclude that, unless strong cancellations occur in the $(Y_\nu^\dagger Y_\nu)_{ij}$ terms, the three observables, $\text{Br}(\mu \rightarrow 3e)$, $\text{Br}(\tau \rightarrow 3e)$ and $\text{Br}(\tau \rightarrow 3\mu)$, are expected to lie within 1 – 2 orders of magnitude. For example, assuming degenerate right-handed neutrinos, a vanishing Dirac phase in the neutrino sector, a normal hierarchy and a vanishing lightest neutrino mass ($m_{\nu_1} = 0$), one finds $\text{Br}(\mu \rightarrow 3e) \sim 70 \text{Br}(\tau \rightarrow 3e) \sim 0.7 \text{Br}(\tau \rightarrow 3\mu)$. An observation of $\tau \rightarrow 3e$ or $\tau \rightarrow 3\mu$ at rates much larger than those expected for $\mu \rightarrow 3e$ could only be accommodated with a strong cancellation in $(Y_\nu^\dagger Y_\nu)_{12}$, that would suppress the $\mu - e$ transitions while still allowing for $\tau - e$ and $\tau - \mu$ LFV¹⁷. Similar results for this observable in an inverse seesaw framework with an extended gauge group have been found in [21]. Finally, in Z -penguin dominated scenarios there is a clear correlation between the rates for $\mu \rightarrow 3e$ and $\mu - e$ conversion in nuclei. Numerically, we find $\text{CR}(\mu - e, \text{Ti})/\text{Br}(\mu \rightarrow 3e) \sim 15$.

5.5 $\tau \rightarrow P^0 \ell_i$

We now address τ flavour violating decays with a light pseudoscalar meson in the final state, $\tau \rightarrow P^0 \ell_i$. As done for the previous observables, we present our results for the branching ratios as a function of M , and for three different values for \hat{M}_R . This can be seen in Figure 7, where we focus on the particular case $\tau \rightarrow \eta \mu$.

We observe in Figure 7 a clear enhancement which is again due to the dominance of the Z -boson mediated contributions in the total amplitude. However the branching ratio remains small as the size of the $(Y_\nu^\dagger Y_\nu)_{23}$ terms never exceeds $O(10^{-2})$.

¹⁷In such a scenario, $\mu - e$ conversion in nuclei and $\mu \rightarrow e\gamma$ would be suppressed as well.

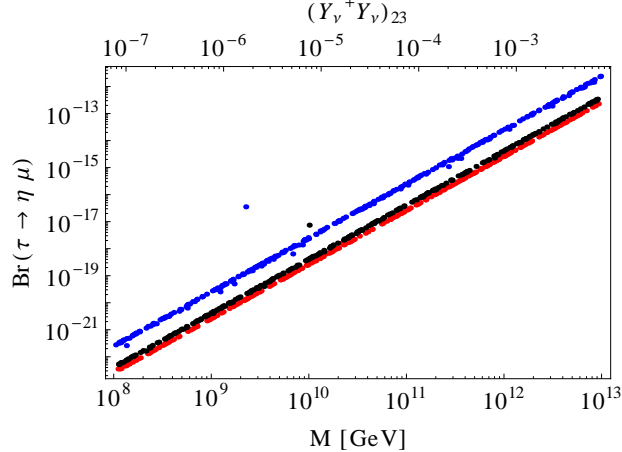


Figure 7: $\text{Br}(\tau \rightarrow \eta\mu)$ as a function of M and $(Y_\nu^\dagger Y_\nu)_{23}$ for different \hat{M}_R values: $\hat{M}_R = 100$ GeV (blue), $\hat{M}_R = 1$ TeV (red) and $\hat{M}_R = 10$ TeV (black). The cMSSM parameters are taken as in figure 5.

In fact, without the Z -penguin contributions, this observable would be much more suppressed (by several orders of magnitude). For example, the Higgs-mediated contributions to this process were studied in [25] and it was found that $\mathcal{O}(1)$ Yukawa couplings would be required to reach observable levels. However, the strong constraints set by $\mu - e$ conversion in nuclei preclude this possibility, implying that $\text{Br}(\tau \rightarrow \eta\mu) \lesssim 10^{-13}$. In conclusion, if the inverse seesaw is realised in Nature, semileptonic τ cLFV decays do not have realistic chances of being observed in the near future unless strong cancellations occur in the $\mu - e$ sector.

Very similar results have been obtained for other mesons, as well as for final states including an electron instead of a muon. These observables also exhibit a very little dependence on the spectrum: large variations in m_0 and $M_{1/2}$ have a minimal impact on the results for $\text{Br}(\tau \rightarrow P^0 \ell_i)$.

5.6 $\ell_i \rightarrow \ell_j \gamma$

Finally, we discuss our results for $\ell_i \rightarrow \ell_j \gamma$. Radiative decays have been intensively studied in the literature (see for instance [9, 48, 68]). However, most of the phenomenological studies have focused only on this observable, neglecting the impact of the Z -boson enhancement on the other cLFV observables. Therefore, our purpose is to determine how the constraints on the parameters of the inverse seesaw extension of the MSSM, derived from the analysis of the Z -boson enhanced observables, affect the predictions for the $\ell_i \rightarrow \ell_j \gamma$ rates. In fact, due to the strong limits on the Yukawa couplings coming from $\mu - e$ conversion in nuclei, $\text{Br}(\ell_i \rightarrow \ell_j \gamma)$ is typically below the experimental limits, the only exception being the $\hat{M}_R = 100$ GeV scenario. This can be seen in Figure 8 where, as expected from theoretical arguments, $\text{Br}(\mu \rightarrow 3e) > \text{Br}(\mu \rightarrow e\gamma)$ in the Z -penguin dominated scenarios¹⁸.

It is also clear from Figure 8 that for low \hat{M}_R , the observable $\text{Br}(\mu \rightarrow e\gamma)$ has very little dependence on m_0 and $M_{1/2}$, whereas for large \hat{M}_R , one can find very large variations due to the different values of the SUSY masses. Similarly, we have checked that the other cMSSM parameters, A_0 , $\tan\beta$, $\text{sign}(\mu)$ and B_0 , do not significantly affect the numerical value of $\text{Br}(\mu \rightarrow e\gamma)$ when $\hat{M}_R = 100$ GeV, but can become relevant for larger values of \hat{M}_R . We find that the non-SUSY

¹⁸This is true for moderate values of m_0 and $M_{1/2}$ or, in other words, when the superparticles running in the loop are reasonably heavy. Similarly, low M_R spoils this feature by increasing the non-SUSY contributions.

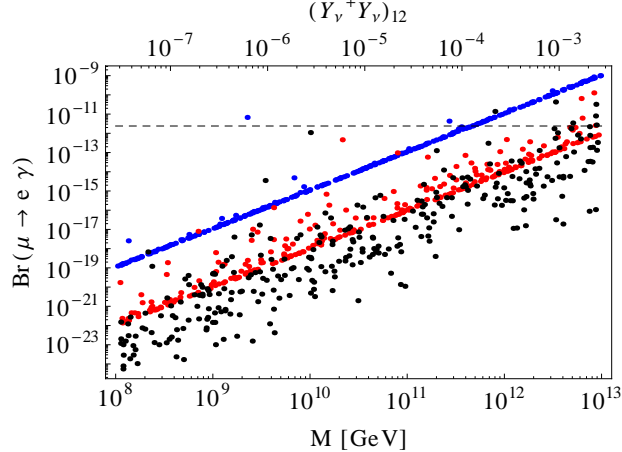


Figure 8: $\text{Br}(\mu \rightarrow e\gamma)$ as a function of M and $(Y_\nu^\dagger Y_\nu)_{12}$ for different \hat{M}_R values: $\hat{M}_R = 100$ GeV (blue), $\hat{M}_R = 1$ TeV (red) and $\hat{M}_R = 10$ TeV (black). The cMSSM parameters are taken as in figure 5. The horizontal dashed line represents the current experimental bound.

contributions to $\text{Br}(\mu \rightarrow e\gamma)$ become relevant only for $\hat{M}_R < 1$ TeV, and in fact, for $\hat{M}_R = 100$ GeV the non-SUSY contributions totally dominate, so that all dependence on m_0 , $M_{1/2}$ and on the rest of cMSSM parameters disappears. These results are in agreement with those found in [9], where it was shown that non-SUSY contributions can enhance $\text{Br}(\ell_i \rightarrow \ell_j\gamma)$ in the inverse seesaw if the singlet fermions are light and have relatively large mixings with the active neutrinos. This result has been confirmed by our numerical study, where we found that $\text{Br}(\ell_i \rightarrow \ell_j\gamma)$ could be enhanced by some orders of magnitude when $\hat{M}_R \ll m_W$. One can thus find regions of the $\hat{M}_R - M$ plane where $\text{Br}(\mu \rightarrow 3e) < \text{Br}(\mu \rightarrow e\gamma)$, contrary to what occurs when SUSY contributions dominate in both observables¹⁹.

5.7 Other observables and benchmark points

To conclude the numerical analysis, we address some aspects not fully covered in the previous sections. We also summarise the most relevant features and results using some specific benchmark points.

Concerning flavour violating neutral boson decays, some additional comments are in order. The cLFV decays of the Z -boson, $Z \rightarrow \ell_i \ell_j$ with $i \neq j$, are not enhanced²⁰ and the corresponding branching ratios lie below experimental reach [87]. Similarly, the branching ratios for $H^0 \rightarrow \ell_i \ell_j$ are very small. This process is known to have a non-decoupling behaviour leading to non-negligible contributions even for very heavy sparticles [44]. However, in the present case, the small Yukawa couplings strongly suppress the corresponding rate. We have also studied collider observables such as $\text{Br}(\tilde{\chi}_2^0 \rightarrow \tilde{\chi}_1^0 \ell_i \ell_j)$ and slepton mass splittings, $\Delta m_{\tilde{\ell}}$. We have found that they have very little relevance in this model as expected from the previous discussion in Section 4.6.

¹⁹The $\hat{M}_R - M$ plane is not only constrained by cLFV observables, but also by Non-Standard Interactions (NSI) [85]. In this model, for degenerate singlets, these bounds can be translated into $\mu_X \gtrsim 20$ eV. This in turn implies that, for a given value of M , one can always find a lower bound on \hat{M}_R . For example, for $M = 10^{12}$ GeV the NSI bound implies $\hat{M}_R \gtrsim 135$ GeV and thus the blue dots in Figure 8 with $M \gtrsim 10^{12}$ GeV, which are ruled out by $\mu \rightarrow e\gamma$, are also disfavoured by NSI. For a non-degenerate spectrum the previous estimate does not hold.

²⁰This process has been studied in detail in [86], where the relevant expressions are given. Recently, good agreement, up to an overall factor of 2 in the wave function contributions, was found in [41].

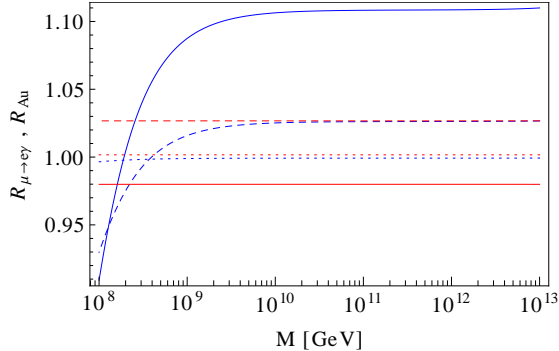


Figure 9: $R_{\mu \rightarrow e\gamma}$ (blue) and R_{Au} (red) as a function of M . The M_R matrix is given by $M_R = \text{diag}(\hat{M}_{R1}, 10 \text{ TeV}, 10 \text{ TeV})$, with $\hat{M}_{R1} = 30 \text{ GeV}$ (solid lines), $\hat{M}_{R1} = 100 \text{ GeV}$ (dashed lines) and $\hat{M}_{R1} = 1 \text{ TeV}$ (dotted lines). The cMSSM parameters take the values $m_0 = 500 \text{ GeV}$, $M_{1/2} = 1 \text{ TeV}$, $A_0 = -300 \text{ GeV}$, $B_0 = 0$ and $\tan \beta = 10$.

For completeness, we briefly discuss the case of non-degenerate right-handed neutrinos, $M_R = \text{diag}(\hat{M}_{R1}, \hat{M}_{R2}, \hat{M}_{R3})$, with $\hat{M}_{Ri} \neq \hat{M}_{Rj}$. In our analysis we considered three different values for \hat{M}_{R1} (30 GeV, 100 GeV and 1 TeV), fixed $\hat{M}_{R2} = \hat{M}_{R3} = 10 \text{ TeV}$ and varied M in the range $[10^8, 10^{13} \text{ GeV}]$. In order to allow for a comparison with the degenerate case (setting, for example, $\hat{M}_{R1} = \hat{M}_{R2} = \hat{M}_{R3} = 10 \text{ TeV}$) and to identify the effect of the right-handed neutrino spectrum on the cLFV observables, we have taken a common M for the three right-handed neutrinos by adjusting the corresponding $\hat{\mu}_{Xi}$. This allows to have identical values for the Yukawa couplings in the degenerate and non-degenerate cases. To better evaluate the difference between the degenerate and non-degenerate cases, we further define the ratios

$$R_{\mu \rightarrow e\gamma} = \frac{\text{Br}(\mu \rightarrow e\gamma)_{\text{non-deg}}}{\text{Br}(\mu \rightarrow e\gamma)_{\text{deg}}} \quad , \quad R_{\text{Au}} = \frac{\text{CR}(\mu - e, \text{Au})_{\text{non-deg}}}{\text{CR}(\mu - e, \text{Au})_{\text{deg}}} \quad . \quad (5.4)$$

The results can be seen in Figure 9 where the cMSSM parameters take the arbitrary (but representative) values $m_0 = 500 \text{ GeV}$, $M_{1/2} = 1 \text{ TeV}$, $A_0 = -300 \text{ GeV}$, $B_0 = 0$ and $\tan \beta = 10$. As expected, $\text{Br}(\mu \rightarrow e\gamma)$ is affected by a change in the singlet spectrum. However, one can see that the relative difference (for this particular choice of parameters) can reach at most $\sim 10\%$. The change in the Z -boson mediated processes is negligible: for example, the relative change in the $\mu - e$ conversion rate in gold is always below 2%, independently of the value of M . This is another example of the little impact that the mass spectrum has on the Z -boson mediated processes. In conclusion, a non-degenerate right-handed neutrino spectrum can indeed induce changes to the observables, but these are typically small and the essence of the results derived here is unaffected by the nature of the right-handed neutrino spectrum²¹.

Finally, we present our results for the cLFV observables for the two benchmark points of Table 2. Point A is associated to a Higgs mass $m_{h^0} = 126.5 \text{ GeV}$, in agreement with the latest LHC [76, 77] and Tevatron [78] results²². We note that, although the inverse seesaw contains additional degrees of freedom beyond those of the cMSSM, the smallness of the Yukawa couplings implies that any correction to the Higgs mass, m_{h^0} , arising from the singlet sector will be very

²¹There is an exception to this general statement: in the non-degenerate case, the R matrix is indeed relevant even if it is real [46].

²²Our numerical routines for the computation of the Higgs mass, based on `SPheno 3.1.9` [69, 70], agree with the results of [79–81], within the usual theoretical uncertainty of $\sim 1 - 2 \text{ GeV}$.

Point	m_0 [TeV]	$M_{1/2}$ [TeV]	A_0 [TeV]	B_0 [TeV]	$\tan \beta$	$\text{sign}(\mu)$
A	0.5	1.5	-3	0	20	+
B	3	3	0	0	10	+

Table 2: Benchmark points used in the numerical analysis. Point A leads to a Higgs mass of $m(h^0) = 126.5$ GeV, in accordance with the latest LHC results. Point B is an example of a very heavy supersymmetric spectrum.

small²³. Point B exemplifies a very heavy supersymmetric spectrum with associated gluino and squark masses larger than 6 TeV and lightest chargino and sneutrino masses of 2.3 TeV and 3 TeV, respectively. It has been selected in order to show explicitly the non-decoupling behaviour of the Z -mediated processes.

The results for the cLFV observables are given in Table 3 and, for completeness, we display in Table 4 the current experimental bounds and future sensitivities for the same cLFV observables. For each point we have taken three different spectra in the singlet sector: (1) $\hat{M}_{R1} = \hat{M}_{R2} = \hat{M}_{R3} = 100$ GeV, (2) $\hat{M}_{R1} = \hat{M}_{R2} = \hat{M}_{R3} = 1$ TeV, and (3) $\hat{M}_{R1} = 50$ GeV, $\hat{M}_{R2} = 500$ GeV, $\hat{M}_{R3} = 1$ TeV. The first case serves to show the influence of the non-SUSY contributions to $\ell_i \rightarrow \ell_j \gamma$, the second one is a standard degenerate scenario where the SUSY contributions dominate all processes, while the third case is a non-degenerate scenario with an intermediate situation. In all cases we fix $M = 4 \times 10^{11}$ GeV.

Firstly, we observe that $\text{Br}(\ell_i \rightarrow \ell_j \gamma)$ shows very little change when going from scenario A-1 (with relatively light sparticles) to B-1 (with very heavy sparticles). As discussed in Section 5.6, in scenarios with very low masses for the right-handed neutrinos, the main contributions to $\text{Br}(\ell_i \rightarrow \ell_j \gamma)$ are non-supersymmetric. Therefore, they are obviously unaffected by the size of the SUSY parameters. We also point out that, although the right-handed neutrinos are light in these two scenarios, the bounds from NSI [85] are satisfied due to the smallness of the Yukawa couplings. Another interesting remark that can be made in association to Table 3 is the different behaviour of the radiative $\ell_i \rightarrow \ell_j \gamma$ and the Z -mediated processes when going from the A-2 point to the B-2 point. While $\text{Br}(\ell_i \rightarrow \ell_j \gamma)$ is clearly reduced, in agreement with the well-known dependence on the SUSY spectrum, $\propto m_{\text{SUSY}}^{-4}$, the rates for the Z -mediated processes hardly change. This is a clear indication of the non-decoupling behaviour due to the Z -penguins. Finally, points A-3 and B-3 show an intermediate case, with one light right-handed neutrino, yielding results quite similar to those in points A-2 and B-2. Thus, as discussed before, the nature of the right-handed neutrinos spectrum is irrelevant.

6 Conclusion

The supersymmetric inverse seesaw is a very attractive extension of the MSSM, with neutrino masses generated by TeV-scale mediators, in association with potentially large Yukawa couplings. In this work, we have studied in detail the predictions for several lepton flavour violating observables, focusing on those mediated by Z -boson exchange. These are particularly interesting when the non-supersymmetric contributions are small.

We have found that, due to the non-decoupling behaviour, the Z -penguins totally dominate the cLFV amplitudes in most of the parameter space, especially in scenarios where the right-handed neutrinos and the supersymmetric particles have masses larger than ~ 500 GeV. In those

²³For large Yukawa coupling, an enhancement to the Higgs mass can be found. However, this is often in conflict with bounds from LFV [88].

cLFV Process	A-1	A-2	A-3	B-1	B-2	B-3
$\mu \rightarrow e\gamma$	1.9×10^{-12}	1.2×10^{-13}	1.3×10^{-13}	1.7×10^{-12}	1.5×10^{-15}	3.6×10^{-15}
$\tau \rightarrow e\gamma$	2.9×10^{-14}	3.6×10^{-15}	3.4×10^{-15}	2.4×10^{-14}	2.1×10^{-17}	8.7×10^{-17}
$\tau \rightarrow \mu\gamma$	2.7×10^{-12}	3.4×10^{-13}	3.3×10^{-13}	2.3×10^{-12}	2.0×10^{-15}	7.7×10^{-16}
$\mu \rightarrow 3e$	2.9×10^{-14}	3.3×10^{-15}	2.7×10^{-15}	3.0×10^{-14}	2.4×10^{-15}	1.8×10^{-15}
$\tau \rightarrow 3e$	5.5×10^{-16}	7.6×10^{-17}	1.3×10^{-16}	5.3×10^{-16}	3.4×10^{-17}	9.2×10^{-17}
$\tau \rightarrow 3\mu$	2.9×10^{-14}	4.4×10^{-15}	4.7×10^{-15}	3.1×10^{-14}	3.2×10^{-15}	3.6×10^{-15}
$\mu - e$, Au	1.2×10^{-13}	3.5×10^{-14}	2.7×10^{-14}	1.4×10^{-13}	2.8×10^{-14}	2.1×10^{-14}
$\mu - e$, Ti	6.7×10^{-14}	2.8×10^{-14}	2.2×10^{-14}	8.4×10^{-14}	2.2×10^{-14}	1.6×10^{-14}
$\tau \rightarrow e\eta$	4.3×10^{-17}	4.5×10^{-18}	1.3×10^{-17}	4.6×10^{-17}	4.7×10^{-18}	1.3×10^{-17}
$\tau \rightarrow \mu\eta$	4.0×10^{-15}	4.2×10^{-16}	4.7×10^{-16}	4.3×10^{-15}	4.3×10^{-16}	4.9×10^{-16}

Table 3: Results for several lepton flavour violating processes for the benchmark points of Table 2 supplemented with three different singlet spectra: (1) $\hat{M}_{R1} = \hat{M}_{R2} = \hat{M}_{R3} = 100$ GeV, (2) $\hat{M}_{R1} = \hat{M}_{R2} = \hat{M}_{R3} = 1$ TeV, and (3) $\hat{M}_{R1} = 50$ GeV, $\hat{M}_{R2} = 500$ GeV, $\hat{M}_{R3} = 1$ TeV.

cLFV Process	Present Bound	Future Sensitivity
$\mu \rightarrow e\gamma$	2.4×10^{-12} [55]	$\mathcal{O}(10^{-13})$ [55]
$\tau \rightarrow e\gamma$	3.3×10^{-8} [89]	3.0×10^{-9} [56]
$\tau \rightarrow \mu\gamma$	4.4×10^{-8} [89]	2.4×10^{-9} [56]
$\mu \rightarrow 3e$	1.0×10^{-12} [28]	$\mathcal{O}(10^{-16})$ [59]
$\tau \rightarrow 3e$	2.7×10^{-8} [57]	2.3×10^{-10} [56]
$\tau \rightarrow 3\mu$	2.1×10^{-8} [57]	8.2×10^{-10} [56]
$\mu - e$, Au	7.0×10^{-13} [61]	
$\mu - e$, Ti	4.3×10^{-12} [60]	$\mathcal{O}(10^{-18})$ [66]
$\tau \rightarrow e\eta$	4.4×10^{-8} [58]	$\mathcal{O}(10^{-10})$ [56]
$\tau \rightarrow \mu\eta$	2.3×10^{-8} [58]	$\mathcal{O}(10^{-10})$ [56]

Table 4: The current experimental bounds and future sensitivities for the cLFV observables.

cases, $\mu - e$ conversion in nuclei is the most constraining observable, clearly more restrictive than $\mu \rightarrow e\gamma$. As a result of the large enhancement provided by the Z -penguins, one can set very strong constraints on the size of the flavour violating couplings.

Finally, we emphasize that the bounds obtained in this work apply to the off-diagonal elements of the Yukawa couplings. One can also set bounds on the diagonal ones using the invisible width of the Z boson. This effect is negligible in our case due to the smallness of the Yukawa couplings.

Acknowledgements

We are grateful to Florian Staub for comments and corrections on the numerical code. A.V. thanks María José Herrero for interesting discussions. D.D. acknowledges financial support from the CNRS. This work has been partly done under the ANR project CPV-LFV-LHC NT09-508531. The authors acknowledge partial support from the European Union FP7 ITN INVISIBLES (Marie Curie Actions, PITN- GA-2011- 289442).

References

- [1] Y. Abe *et al.* [DOUBLE-CHOOZ Collaboration], Phys. Rev. Lett. **108** (2012) 131801 [arXiv:1112.6353 [hep-ex]].
- [2] M. Hartz [T2K Collaboration], arXiv:1201.1846 [hep-ex].
- [3] P. Adamson *et al.* [MINOS Collaboration], Phys. Rev. Lett. **108** (2012) 191801 [arXiv:1202.2772 [hep-ex]].
- [4] F. P. An *et al.* [DAYA-BAY Collaboration], Phys. Rev. Lett. **108** (2012) 171803 [arXiv:1203.1669 [hep-ex]].
- [5] J. K. Ahn *et al.* [RENO collaboration], Phys. Rev. Lett. **108** (2012) 191802 [arXiv:1204.0626 [hep-ex]].
- [6] D. V. Forero, M. Tortola and J. W. F. Valle, arXiv:1205.4018 [hep-ph].
- [7] G. L. Fogli, E. Lisi, A. Marrone, D. Montanino, A. Palazzo and A. M. Rotunno, arXiv:1205.5254 [hep-ph].
- [8] R. N. Mohapatra and J. W. F. Valle, Phys. Rev. D **34** (1986) 1642.
- [9] F. Deppisch and J. W. F. Valle, Phys. Rev. D **72** (2005) 036001 [arXiv:hep-ph/0406040].
- [10] F. Deppisch, T. S. Kosmas and J. W. F. Valle, Nucl. Phys. B **752** (2006) 80 [arXiv:hep-ph/0512360].
- [11] J. Garayoa, M. C. Gonzalez-Garcia and N. Rius, JHEP **0702** (2007) 021 [hep-ph/0611311].
- [12] C. Arina, F. Bazzocchi, N. Fornengo, J. C. Romao and J. W. F. Valle, Phys. Rev. Lett. **101** (2008) 161802 [arXiv:0806.3225 [hep-ph]].
- [13] E. Ma, Phys. Rev. D **80** (2009) 013013 [arXiv:0904.4450 [hep-ph]].
- [14] P. S. B. Dev and R. N. Mohapatra, Phys. Rev. D **81** (2010) 013001 [arXiv:0910.3924 [hep-ph]].
- [15] M. Malinsky, T. Ohlsson, Z. -z. Xing and H. Zhang, Phys. Lett. B **679** (2009) 242 [arXiv:0905.2889 [hep-ph]].
- [16] F. Bazzocchi, D. G. Cerdeno, C. Munoz and J. W. F. Valle, Phys. Rev. D **81** (2010) 051701 [arXiv:0907.1262 [hep-ph]].
- [17] M. Hirsch, T. Kernreiter, J. C. Romao and A. Villanova del Moral, JHEP **1001** (2010) 103 [arXiv:0910.2435 [hep-ph]].
- [18] F. Bazzocchi, Phys. Rev. D **83** (2011) 093009 [arXiv:1011.6299 [hep-ph]].
- [19] M. E. Catano, R. Martinez and F. Ochoa, arXiv:1206.1966 [hep-ph].
- [20] A. G. Dias, C. A. de S.Pires, P. S. Rodrigues da Silva and A. Sampieri, arXiv:1206.2590 [hep-ph].
- [21] M. Hirsch, W. Porod, L. Reichert and F. Staub, arXiv:1206.3516 [hep-ph].

- [22] S. Mondal, S. Biswas, P. Ghosh and S. Roy, JHEP **1205** (2012) 134 [arXiv:1201.1556 [hep-ph]].
- [23] P. S. B. Dev, R. Franceschini and R. N. Mohapatra, arXiv:1207.2756 [hep-ph].
- [24] A. Das and N. Okada, arXiv:1207.3734 [hep-ph].
- [25] A. Abada, D. Das and C. Weiland, JHEP **1203** (2012) 100 [arXiv:1111.5836 [hep-ph]].
- [26] B. Aubert *et al.* [BABAR Collaboration], Phys. Rev. Lett. **96** (2006) 041801 [hep-ex/0508012].
- [27] B. Aubert *et al.* [BABAR Collaboration], Phys. Rev. Lett. **95** (2005) 041802 [hep-ex/0502032].
- [28] U. Bellgardt *et al.* [SINDRUM Collaboration], Nucl. Phys. B **299** (1988) 1.
- [29] B. Aubert *et al.* [BABAR Collaboration], Phys. Rev. Lett. **92** (2004) 121801 [hep-ex/0312027].
- [30] A. G. Akeroyd *et al.* [SuperKEKB Physics Working Group Collaboration], hep-ex/0406071.
- [31] Y. Kuno, Nucl. Phys. Proc. Suppl. **149** (2005) 376.
- [32] O. A. Kiselev [MEG Collaboration], Nucl. Instrum. Meth. A **604** (2009) 304.
- [33] S. Ritt [MEG Collaboration], Nucl. Phys. Proc. Suppl. **162** (2006) 279.
- [34] K. Hayasaka *et al.* [Belle Collaboration], Phys. Lett. B **666** (2008) 16 [arXiv:0705.0650 [hep-ex]].
- [35] A. Abada, A. J. R. Figueiredo, J. C. Romao and A. M. Teixeira, JHEP **1010** (2010) 104 [arXiv:1007.4833 [hep-ph]].
- [36] J. N. Esteves, J. C. Romao, M. Hirsch, A. Vicente, W. Porod and F. Staub, JHEP **1012** (2010) 077 [arXiv:1011.0348 [hep-ph]].
- [37] A. Abada, A. J. R. Figueiredo, J. C. Romao and A. M. Teixeira, JHEP **1108** (2011) 099 [arXiv:1104.3962 [hep-ph]].
- [38] A. Abada, A. J. R. Figueiredo, J. C. Romao and A. M. Teixeira, arXiv:1206.2306 [hep-ph].
- [39] E. Arganda, M. J. Herrero and A. M. Teixeira, JHEP **0710** (2007) 104 [arXiv:0707.2955 [hep-ph]].
- [40] M. Hirsch, F. Staub and A. Vicente, arXiv:1202.1825 [hep-ph].
- [41] H. K. Dreiner, K. Nickel, F. Staub and A. Vicente, arXiv:1204.5925 [hep-ph].
- [42] A. M. Curiel, M. J. Herrero and D. Temes, Phys. Rev. D **67** (2003) 075008 [arXiv:hep-ph/0210335].
- [43] A. M. Curiel, M. J. Herrero, W. Hollik, F. Merz and S. Penaranda, Phys. Rev. D **69** (2004) 075009 [arXiv:hep-ph/0312135].
- [44] E. Arganda, A. M. Curiel, M. J. Herrero and D. Temes, Phys. Rev. D **71** (2005) 035011 [arXiv:hep-ph/0407302].
- [45] M. C. Gonzalez-Garcia and J. W. F. Valle, Phys. Lett. B **216** (1989) 360.

- [46] J. A. Casas and A. Ibarra, Nucl. Phys. B **618** (2001) 171 [arXiv:hep-ph/0103065].
- [47] T. Schwetz, M. Tortola and J. W. F. Valle, New J. Phys. **13** (2011) 063004 [arXiv:1103.0734 [hep-ph]].
- [48] J. Hisano, T. Moroi, K. Tobe and M. Yamaguchi, Phys. Rev. D **53** (1996) 2442 [arXiv:hep-ph/9510309].
- [49] E. Arganda and M. J. Herrero, Phys. Rev. D **73** (2006) 055003 [arXiv:hep-ph/0510405].
- [50] K. S. Babu and C. Kolda, Phys. Rev. Lett. **89** (2002) 241802 [arXiv:hep-ph/0206310].
- [51] E. Lunghi, A. Masiero, I. Scimemi and L. Silvestrini, Nucl. Phys. B **568** (2000) 120 [arXiv:hep-ph/9906286].
- [52] E. Arganda, M. J. Herrero and J. Portoles, JHEP **0806** (2008) 079 [arXiv:0803.2039 [hep-ph]].
- [53] T. Appelquist and J. Carazzone, Phys. Rev. D **11** (1975) 2856.
- [54] E. Katehou and G. G. Ross, Nucl. Phys. B **299** (1988) 484.
- [55] J. Adam *et al.* [MEG collaboration], Phys. Rev. Lett. **107** (2011) 171801 [arXiv:1107.5547 [hep-ex]].
- [56] B. O’Leary *et al.* [SuperB Collaboration], arXiv:1008.1541 [hep-ex].
- [57] K. Hayasaka *et al.*, Phys. Lett. B **687** (2010) 139 [arXiv:1001.3221 [hep-ex]].
- [58] K. Hayasaka [Belle Collaboration], PoS **ICHEP2010** (2010) 241 [arXiv:1011.6474 [hep-ex]].
- [59] A. Blondel *et al.*, http://www.psi.ch/mu3e/DocumentsEN/LOI_Mu3e_PSI.pdf
- [60] C. Dohmen *et al.* [SINDRUM II Collaboration], Phys. Lett. B **317** (1993) 631.
- [61] W. Bertl *et al.* [SINDRUM II Collaboration], Eur. Phys. J. **C47** (2006) 337-346
- [62] D. Glenzinski [Mu2e Collaboration], AIP Conf. Proc. **1222** (2010) 383.
- [63] R. M. Carey *et al.* [Mu2e Collaboration], FERMILAB-PROPOSAL-0973.
- [64] M. Aoki [DeeMe Collaboration], PoS **ICHEP 2010** (2010) 279.
- [65] Y. G. Cui *et al.* [COMET Collaboration], KEK-2009-10.
- [66] The PRIME working group, unpublished; LOI to J-PARC 50-GeV PS, LOI-25, <http://www-ps.kek.jp/jhf-np/LOIlist/pdf/L25.pdf>
- [67] H. C. Chiang, E. Oset, T. S. Kosmas, A. Faessler and J. D. Vergados, Nucl. Phys. A **559** (1993) 526.
- [68] J. Hisano, T. Moroi, K. Tobe, M. Yamaguchi and T. Yanagida, Phys. Lett. B **357** (1995) 579 [hep-ph/9501407].
- [69] W. Porod, Comput. Phys. Commun. **153** (2003) 275 [arXiv:hep-ph/0301101].
- [70] W. Porod and F. Staub, arXiv:1104.1573 [hep-ph].

- [71] F. Staub, T. Ohl, W. Porod and C. Speckner, arXiv:1109.5147 [hep-ph].
- [72] F. Staub, Comput. Phys. Commun. **182** (2011) 808 [arXiv:1002.0840 [hep-ph]].
- [73] F. Staub, Comput. Phys. Commun. **181** (2010) 1077 [arXiv:0909.2863 [hep-ph]].
- [74] W. Abdallah, A. Awad, S. Khalil and H. Okada, arXiv:1105.1047 [hep-ph].
- [75] R. Lal Awasthi and M. K. Parida, arXiv:1112.1826 [hep-ph].
- [76] G. Aad *et al.* [ATLAS Collaboration], Phys. Lett. B **710** (2012) 49 [arXiv:1202.1408 [hep-ex]].
- [77] S. Chatrchyan *et al.* [CMS Collaboration], Phys. Lett. B **710** (2012) 26 [arXiv:1202.1488 [hep-ex]].
- [78] [TEVNPH (Tevatron New Phenomina and Higgs Working Group) and CDF and D0 Collaborations], arXiv:1203.3774 [hep-ex].
- [79] A. Arbey, M. Battaglia, A. Djouadi, F. Mahmoudi and J. Quevillon, Phys. Lett. B **708** (2012) 162 [arXiv:1112.3028 [hep-ph]].
- [80] H. Baer, V. Barger and A. Mustafayev, dark matter searches,” Phys. Rev. D **85** (2012) 075010 [arXiv:1112.3017 [hep-ph]].
- [81] J. Ellis and K. A. Olive, Eur. Phys. J. C **72** (2012) 2005 [arXiv:1202.3262 [hep-ph]].
- [82] A. Elsayed, S. Khalil and S. Moretti, arXiv:1106.2130 [hep-ph].
- [83] G. Aad *et al.* [ATLAS Collaboration], Phys. Lett. B **710** (2012) 67 [arXiv:1109.6572 [hep-ex]].
- [84] S. Chatrchyan *et al.* [CMS Collaboration], Phys. Rev. Lett. **107** (2011) 221804 [arXiv:1109.2352 [hep-ex]].
- [85] S. Antusch, J. P. Baumann and E. Fernandez-Martinez, Nucl. Phys. B **810** (2009) 369 [arXiv:0807.1003 [hep-ph]].
- [86] X. J. Bi, Y. B. Dai and X. Y. Qi, Phys. Rev. D **63** (2001) 096008 [arXiv:hep-ph/0010270].
- [87] K. Nakamura *et al.* [Particle Data Group], J. Phys. G **37** (2010) 075021.
- [88] M. Hirsch, M. Malinsky, W. Porod, L. Reichert and F. Staub, JHEP **1202** (2012) 084 [arXiv:1110.3037 [hep-ph]].
- [89] B. Aubert *et al.* [BABAR Collaboration], Phys. Rev. Lett. **104** (2010) 021802 [arXiv:0908.2381 [hep-ex]].